Theor. Comput. Fluid Dyn. (2018) 32: 137–164
https://doi.org/10.1007/s00162-017-0443-z

ORIGINAL ARTICLE

Sabine Hittmeir · Rupert Klein

Asymptotics for moist deep convection I: refined scalings and self-sustaining updrafts

Received: 14 April 2017 / Accepted: 22 August 2017 Published online: 5 October 2017

Abstract Moist processes are among the most important drivers of atmospheric dynamics, and scale analysis and asymptotics are cornerstones of theoretical meteorology. Accounting for moist processes in systematic scale analyses therefore seems of considerable importance for the field. Klein and Majda (Theor Comput Fluid Dyn 20:525–551, 2006) proposed a scaling regime for the incorporation of moist bulk microphysics closures in multiscale asymptotic analyses of tropical deep convection. This regime is refined here to allow for mixtures of ideal gases and to establish consistency with a more general multiple scales modeling framework for atmospheric flows. Deep narrow updrafts, the so-called hot towers, constitute principal building blocks of larger scale storm systems. They are analyzed here in a sample application of the new scaling regime. A single quasi-one-dimensional upright columnar cloud is considered on the vertical advective (or tower life cycle) time scale. The refined asymptotic scaling regime is essential for this example as it reveals a new mechanism for the self-sustainance of such updrafts. Even for strongly positive convectively available potential energy, a vertical balance of buoyancy forces is found in the presence of precipitation. This balance induces a diagnostic equation for the vertical velocity, and it is responsible for the generation of self-sustained balanced updrafts. The time-dependent updraft structure is encoded in a Hamilton–Jacobi equation for the precipitation mixing ratio. Numerical solutions of this equation suggest that the self-sustained updrafts may strongly enhance hot tower life cycles.

Keywords Moist atmospheric flows · Multiscale asymptotics · Matched asymptotic expansions · Hot towers · Cumulonimbus clouds

1 Introduction

Solutions to the full governing equations for atmospheric flows are analytically and numerically challenging and often difficult to interpret. Model reductions by scale analysis provide important complementary insights and therefore have a long history in meteorology. One key technique that allows for systematic studies of complex process interactions across disparate length and time scales is multiple scales asymptotics.

Of particular interest in meteorology are multiscale interactions involving moist physics processes. A bulk microphysics closure for the moisture dynamics was first successfully incorporated into an asymptotics

Communicated by William Dewar.

S. Hittmeir
University of Vienna, Vienna, Austria
E-mail: sabine.hittmeir@univie.ac.at

R. Klein (✉)
Freie Universität Berlin, Berlin, Germany
E-mail: rupert.klein@math.fu-berlin.de

framework by [1]. The warm cloud moisture model used in that study consists of balance equations for water vapor, cloud water, and rain water, with phase exchange terms corresponding to the basic "Kessler scheme," [2]. This type of parameterization has been widely used in various variants and generalizations in meteorological modeling, see also [3–7].

A prerequisite for multiple scales analyses is that all of the participating scale-dependent phenomena are represented within one common asymptotic scaling regime or distinguished limit [8]. The moist process scaling regime introduced in [1] is suitable for the purpose of studying the short-time evolution of hot convective cloud towers, but it is not fully consistent with the broadly applicable, unified asymptotic modeling framework developed in parallel and summarized in [8]. It also neglects the individual thermodynamic properties of the moisture species.

The first goal of the present work is therefore to redefine the asymptotic regime for moist physics so as to reconcile it with the general framework and to make it applicable, thereby, to more general atmospheric flow situations. At the same time, we allow for more realistic thermodynamics by including mixtures of ideal gases and state-dependent latent heat.

Latent heat conversion due to phase changes of water in the atmosphere strongly influences its energy balance. Of particular interest here are "hot towers," *i.e.*, large deep convective cumulonimbus clouds that occupy small horizontal scales with typical diameters of a kilometer, see [9,10]. It is a common belief that these hot towers are to a great extent responsible for the vertical energy transport to the upper troposphere within the intertropical convergence zone (see also [10–12] and references therein). Moreover, they are the building blocks of intermediate scale convective storms, [13].

Using asymptotic techniques, a multiscale model for the short-time evolution of hot towers and their interaction with internal waves was developed in [1]. That work also forms the basis for subsequent investigations in [14,15]. These reveal that moisture can reduce the vertical energy transport by internal gravity waves, which may be of considerable importance for climate models. The internal wave time scale considered in that study is much shorter, however, than the time scale of vertical convection in a cloud tower or than the overall cloud tower life cycle time scale. As a consequence, the asymptotic regime considered in [1] is not appropriate for studying cloud dynamics in the context of, for example, self-organized convection and the formation of strong storm fronts (squall lines) or the development of an atmospheric vortex.

The second goal of the present work is, therefore, to reconsider the asymptotics of narrow deep convective hot towers on time scales comparable to the vertical advection time within a tower. An individual, essentially isolated and upright cloud tower is analyzed here as an example for applications of the new asymptotic scaling regime. The effect on individual tower dynamics of the tilt resulting from vertical shear of the background flow as well as interactions between towers in multicellular convection will be addressed in future work. In combination with the refined moist physics closure scheme, we find on this larger time scale an interesting and apparently new regime of self-sustained precipitation-driven convection.

The outline of the rest of the paper is as follows. The remainder of this introduction briefly summarizes the main results of the paper. Section 2 introduces the governing equations for cloudy air, which are then rendered dimensionless in Sect. 3. That section also summarizes two distinguished limits for the moist variables: One is pragmatically defined just on the basis of bare magnitudes of various thermodynamics parameters, and the other is derived from a detailed scale analysis of the hydrostatic moist adiabatic distribution in Sect. 4. The governing equations are reconsidered in Sect. 5 based on an asymptotic ansatz for narrow cloud towers, and the tower evolution equations on the convective time scale for saturated and undersaturated regions are derived through boundary layer-type asymptotic arguments. Slight differences between the two asymptotic scaling regimes from Sect. 3 are discussed. Section 6 provides sample numerical solutions of the new convective time scale tower dynamics equations to reveal the essential physical mechanisms they encode. The potential for self-sustainance of precipitating deep convective updrafts is discussed, in particular. We close with a summary and further discussion in Sect. 7.

1.1 Summary of the main results

1.1.1 Asymptotic scaling regimes for moist air thermodynamics

The thermodynamic characteristics of moist air are captured by the equation of state parameters summarized in Table 1. Together with a reference temperature, T_{ref}, there are seven dimensional quantities of influence involving the two independent physical dimensions of specific energy, measured in units of J/kg, and temperature, measured in K, and this gives rise to five independent dimensionless parameters as listed in Table 2.

Table 1 Thermodynamic equation of state parameters for moist air at reference temperature $T_{\text{ref}} = 273.15$ K (see, for example, [3,5])

c_{pd}	1005	J/kg/K	Dry air specific heat capacity at constant pressure
R_d	287	J/kg/K	Dry air gas constant
c_{pv}	1850	J/kg/K	Water vapor specific heat capacity at constant pressure
R_v	462	J/kg/K	Water vapor gas constant
c_l	4218	J/kg/K	Liquid water specific heat capacity
L_{ref}	2.5×10^6	J/kg	Latent heat of condensation at reference conditions

Table 2 Approximate values and scalings of dimensionless thermodynamics parameters

	Value	Regime $\alpha = 0$	Regime $\alpha = 1$
Parameters			
$\frac{R_d}{c_{\text{pd}}}$	0.29	$\varepsilon\Gamma$	$\varepsilon\Gamma$
$\frac{c_{\text{pv}}}{c_{\text{pd}}}$	1.8	$\varepsilon^{-1}k_v$	k_v
$\frac{R_v}{c_{\text{pd}}}$	0.46	$1/A$	$1/A$
$\frac{c_l}{c_{\text{pd}}}$	4.2	$\varepsilon^{-1}k_l$	$\varepsilon^{-1}k_l$
$\frac{L_{\text{ref}}}{c_{\text{pd}}}T_{\text{ref}}$	9.1	$\varepsilon^{-1}L$	$\varepsilon^{-1}L$
Derived parameters			
$\frac{R_d}{R_v}$	0.62	εE	E
$\frac{c_{\text{pv}}}{c_{\text{pd}}}\frac{R_d}{c_{\text{pd}}} - \frac{R_v}{c_{\text{pd}}}$	0.067	κ_v	$\varepsilon\kappa_v$

The quantities $\Gamma, k_v, A, k_l, L, E, \kappa_v$ are considered to be constants of order $\mathcal{O}(1)$ as $\varepsilon \to 0$

Table 2 also lists two new scaling regimes for these parameters that we suggest for use in subsequent asymptotic analyses of (warm) moist air flow processes. (Note that we defer the explicit modeling of the ice phase to future work, see Remark 1 below.) The first regime, labeled $\alpha = 0$, is consistent with similarity theory in the sense that we *first* identify a set of dimensionless parameters for the system at hand and *then* introduce a coupled limit between these parameters to enable asymptotic analyses. This limit is shown to (1) embed the asymptotics of moist air systematically within the general modeling framework reported upon in [8] and to (2) constitute a "rich limit" in the sense that a maximum of the effects of water vapor on the equation of state of moist air are maintained at leading and first order. A somewhat awkward feature of this limit is, however, that the scalings in terms of the small parameter ε do not match well in all cases with the actual numbers the dimensionless parameters take for moist air.

The second regime, in contrast, has been defined purely on the basis of the actual magnitudes of the dimensionless parameters. Numbers between 0.4 and 3.0 are considered of order unity, while smaller or larger values are associated with asymptotic rescalings in terms of ε. This provides a scaling that better matches with the actual numbers than the first regime, but it is not strictly consistent with similarity theory. Although this is at odds with the usual procedures, it may actually open up an interesting route of investigation. The thermodynamics of moist air may just be asymptotically compatible with a family of equation systems that features the same functional forms in the constitutive equations as those of moist air, but whose set of determining parameters is less constrained. The results of Sect. 4.2, in which we compare asymptotic and error-controlled numerical approximations to the moist adiabatic distribution, corroborate this point of view.

1.1.2 Reduced dynamical models for up- and downdrafts

Updrafts in saturated air: Under the moist physics closure with refined thermodynamics and on the vertical advective time scale a dominant balance of forces is found in the vertical momentum equation. Positive buoyancy due to a potential temperature perturbation, $\tilde{\theta}$, which results from positive convectively available

potential energy (CAPE), is neutralized by the influence of the water vapor and rain water mixing ratios q_v and q_r onto the effective buoyancy force. In the precipitating core of a cloud tower we have, for the pragmatically defined distinguished limit for the cloud variables,

$$\tilde{\theta} + \left(\frac{1}{E} - 1\right)\left(\overline{q}_{\mathrm{vs}} - \overline{q}_v\right) - q_r = 0, \tag{1}$$

where $\overline{q}_{\mathrm{vs}}(z)$ and $\overline{q}_v(z)$ are the saturation water vapor mixing ratio attained in the convective core and the mean water vapor content in the environment of the hot tower, respectively. These depend on the vertical coordinate, z, only. We recall that mixing ratios by definition compare the density of the gas component to the density of dry air. Moreover, $E = R_d/R_v$ is the ratio of the dry air and vapor gas constants (see Table 2). Cloud water does not enter the buoyancy term to leading order, since it is one order of magnitude smaller than the other moisture components.

The balance equation (1) results from the vertical momentum equation in a similar fashion as the hydrostatic balance for larger scale flows. One might then expect the vertical pressure gradient to be part of the equation. Yet, since we consider narrow vertical convective towers, the pressure is imposed on the column from the side, just as the pressure is imposed from the farfield in ordinary boundary layer theory. Therefore, the pressure cannot adjust individually in each convective tower to balance the buoyancy. Instead, positive contributions to buoyancy from potential temperature fluctuations and the equation of state effect of water vapor and negative contributions from the weight of liquid water can cancel to leading order, and this is expressed in (1).

Next we note that $\tilde{\theta}$ and q_r at the same time satisfy the transport equations

$$D_t q_r - \frac{1}{\overline{\rho}}\partial_z(\overline{\rho} V_r q_r) = -w\,\frac{\mathrm{d}\overline{q}_{\mathrm{vs}}}{\mathrm{d}z} + \mathcal{D}_{q_r} \tag{2}$$

$$D_t\tilde{\theta} = w\frac{\mathrm{d}\Delta\overline{\theta}}{\mathrm{d}z} - k_l q_r(w - V_r)\frac{\mathrm{d}T^{(1)}}{\mathrm{d}z} + \mathcal{D}_\theta \tag{3}$$

where D_t is the total time derivative, $\overline{\rho}$ is the background density, $\Delta\overline{\theta}$ is the second-order difference between the moist adiabatic and the background potential temperature stratifications, V_r is the terminal droplet sedimentation velocity, w is the vertical flow velocity, k_l is a scaled ratio of the specific heats of liquid water and dry air, and $T^{(1)}$ is the first-order temperature stratification. For the terminal sedimentation velocity we follow [1] and adopt the simplest possible approach, which is to assume that $V_r = \text{const.}$ and of the order of a few meters per second. The general source terms $\mathcal{D}_\theta$ and $\mathcal{D}_{q_r}$ represent entrainment due to lateral turbulent transport and related effects. Neglecting these latter terms to focus just on the vertical balances, and combining the balance from (1) and the transport equations in (2) one finds a diagnostic relation for the vertical velocity,

$$\begin{aligned} &w\left(k_l q_r\frac{\mathrm{d}T^{(1)}}{\mathrm{d}z} + \frac{\mathrm{d}\Delta\overline{\theta}}{\mathrm{d}z} - \frac{1}{E}\frac{\mathrm{d}\overline{q}_{\mathrm{vs}}}{\mathrm{d}z} + \left(\frac{1}{E} - 1\right)\frac{\mathrm{d}\overline{q}_v}{\mathrm{d}z}\right) \\ &\quad = k_l q_r V_r\frac{\mathrm{d}T^{(1)}}{\mathrm{d}z} - \frac{1}{\overline{\rho}}\partial_z(\overline{\rho} V_r q_r) \end{aligned} \tag{4}$$

which holds as long as $w > 0$, while the leading order vertical velocity is zero otherwise within the precipitating core. Thus, we have

$$w = W(\partial_z q_r, q_r, z) := \max\left(0,\, A(q_r, z)\, q_r - B(q_r, z)\,\partial_z q_r\right) \tag{5}$$

where $A(q_r, z)$, $B(q_r, z)$ are straightforward abbreviations for terms from (4).

Inserting into (2) and neglecting horizontal transport in a quasi-one-dimensional approximation we find a Hamilton–Jacobi-type equation for the scaled precipitation mixing ratio,

$$\partial_t q_r = -W(\partial_z q_r, q_r, z)\left[\partial_z q_r + \frac{\mathrm{d}\overline{q}_{\mathrm{vs}}}{\mathrm{d}z}\right] + \frac{1}{\overline{\rho}}\,\partial_z\left(\overline{\rho} V_r q_r\right). \tag{6}$$

Numerical solutions to this equation are discussed in Sect. 6 below.

Downdrafts in undersaturated air: Here we consider evaporation-induced downdrafts that arise when rain coming from higher altitudes reaches unsaturated air somewhere in the bulk of the troposphere. The rain could come from anvil clouds residing aloft or from tilted precipitating columns. We are not addressing precipitation below cloud base in the near-surface boundary layer here, but hope to address this scenario in future work.

In the considered undersaturated regions, all cloud water rapidly evaporates, so that its mixing ratio q_c vanishes to leading order. Rain water, in contrast, evaporates at a rate of order unity on the convective time scale, so that the mixing ratios for vapor and rain, q_v, q_r, to leading order satisfy the transport equations

$$\begin{aligned} D_t q_v &= S_{\text{ev}} \\ D_t q_r - \frac{1}{\rho}\partial_z(\rho V_r q_r) &= -S_{\text{ev}} \end{aligned} \qquad \text{with} \qquad S_{\text{ev}} = LC_{\text{ev}}(q_{\text{vs}} - q_v)q_r. \tag{7}$$

The stability associated near moist adiabatic stratification is overcome in undersaturated regions only by evaporative cooling. The vertical velocity then follows the "weak temperature gradient approximation" [1,16, 17],

$$w^{(0)}\frac{\mathrm{d}\theta^{(1)}}{\mathrm{d}z} = -LS_{\text{ev}}^{(0)}. \tag{8}$$

Equations (7) and (8), again in the quasi-1D approximation, constitute the tower model for undersaturated air. Numerical solutions to these undersaturated tower equations are also discussed in Sect. 6 below.

Remark 1 (Ice phase) In this work we do not consider the ice phase of the condensate, since the bulk microphysics model would get much more involved and in particular require to take into account different saturation mixing ratios. Therefore, the further incorporation of solid particles is left for future work. For the convective cores of tropical cumulonimbus clouds and squall lines, however, realistic results have been obtained from warm cloud models, see, for example, [18–20], which clearly does not hold true for stratiform cloud regions in the upper troposphere. For hot towers in particular we expect the ice phase to have some effect on the upper cloud layer, since, as has been pointed out by Zipser [12], the ice phase reinvigorates the updrafts in the upper troposphere and allows them to reach the tropical tropopause.

2 Governing equations

To describe the flow of moist air in the atmosphere we adopt the compressible flow equations with a bulk microphysics closure scheme borrowing from [3,21,22]. We work with the dry air mass-averaged velocity, $\boldsymbol{v}$, such that the dry air mass balance reads

$$\partial_t \rho_d + \nabla\cdot(\rho_d \boldsymbol{v}) = 0, \tag{9}$$

where ρ_d is the dry air mass density. Of the three moisture components, vapor, cloud water, and rain water, we assume the former two to be advected by the dry air flow velocity, $\boldsymbol{v}$, whereas the rain water component falls at the terminal sedimentation velocity V_r.

Based on these preliminaries, the total mass, momentum, potential temperature, and moisture species balances read

$$\partial_t \rho_d + \nabla\cdot(\rho_d \boldsymbol{v}) = 0 \tag{10}$$

$$D_t \boldsymbol{u} + (2\boldsymbol{\Omega}\times\boldsymbol{v})_{\parallel} + \frac{1}{\rho}\nabla_{\parallel} p = \frac{\rho_d}{\rho} q_r V_r \partial_z \boldsymbol{u} + \mathcal{D}_{\boldsymbol{u}} \tag{11}$$

$$D_t w + (2\boldsymbol{\Omega}\times\boldsymbol{v})_{\perp} + \frac{1}{\rho}\partial_z p = -g + \frac{\rho_d}{\rho} q_r V_r \partial_z w + \mathcal{D}_w \tag{12}$$

$$C D_t \ln\theta + \Sigma D_t \ln p + \frac{L(T)}{T} D_t q_v = c_l q_r V_r \left(\partial_z \ln\theta + \frac{R_d}{c_{\text{pd}}}\partial_z \ln p\right) + \mathcal{D}_\theta \tag{13}$$

$$D_t q_v = S_{\text{ev}} - S_{\text{cd}} + \mathcal{D}_{q_v} \tag{14}$$

$$D_t q_c = S_{\text{cd}} - S_{\text{ac}} - S_{\text{cr}} + \mathcal{D}_{q_c} \tag{15}$$

$$D_t q_r - \frac{1}{\rho_d}\partial_z(\rho_d q_r V_r) = S_{\text{ac}} + S_{\text{cr}} - S_{\text{ev}} + \mathcal{D}_{q_r} \tag{16}$$

where

$$\rho = \rho_d\,(1 + q_v + q_c + q_r) \tag{17}$$

$$p = \rho_d R_d T \left(1 + \frac{q_v}{E}\right) \tag{18}$$

$$T = \theta \left(\frac{p}{p_{\text{ref}}}\right)^{\frac{\gamma-1}{\gamma}} \tag{19}$$

$$\boldsymbol{v} = \boldsymbol{u} + w\boldsymbol{k} \tag{20}$$

$$C = c_{\text{pd}} + c_{\text{pv}} q_v + c_l (q_c + q_r) \tag{21}$$

$$\Sigma = \left(\frac{c_{\text{pv}}}{c_{\text{pd}}} R_d - R_v\right) q_v + \frac{c_l}{c_{\text{pd}}} R_d (q_c + q_r) \tag{22}$$

In these equations $(\rho, T, \theta, p, \boldsymbol{u}, w, q_v, q_c, q_r)$ are the density, temperature, potential temperature, pressure, the horizontal and vertical velocity components, and the mixing ratios of water vapor, cloud water, and rain water, respectively, g is the gravitational acceleration, $\boldsymbol{\Omega}$ denotes the Earth rotation vector, and the subscripts $_\perp$ and $_\parallel$ refer to vertical and horizontal components, respectively. The turbulent and molecular transport terms are indicated by $\mathcal{D}$'s. Furthermore, $(c_{\text{pd}}, c_{\text{pv}})$ are the specific heat capacities at constant pressure of dry air and water vapor, c_l is the heat capacity of liquid water, (R_d, R_v) are the dry air and water vapor gas constants, $\gamma = c_{\text{pd}}/(c_{\text{pd}} - R_d)$ is the isentropic exponent of dry air, $\boldsymbol{k}$ is the vertical unit vector, $p_{\text{ref}} = 10^5$ Pa is a reference pressure, and the Lagrangian time derivative is

$$D_t = \partial_t + \boldsymbol{v}\cdot\nabla = \partial_t + \boldsymbol{u}\cdot\nabla_\parallel + w\partial_z. \tag{23}$$

In this work we assume constant heat capacity, c_{pd} and c_l, of dry air and liquid water, which implies that the latent heat of condensation L is linear in the temperature

$$L(T) = L_{\text{ref}} + (c_{\text{pv}} - c_l)(T - T_{\text{ref}}) \equiv L_{\text{ref}}\phi(T). \tag{24}$$

The source terms $S_{\text{ev}}, S_{\text{cd}}, S_{\text{ac}}, S_{\text{cr}}$ are the rates of evaporation of rain water, the condensation of water vapor to cloud water and the inverse evaporation process, the autoconversion of cloud water into rainwater by accumulation of microscopic droplets, and the collection of cloud water by falling rain. To close the moisture dynamics we adopt the setting of [1] corresponding to a basic form of the bulk microphysics closure in the spirit of Kessler [2] and Grabowski and Smolarkiewicz [6]:

$$S_{\text{cd}} = C_{\text{cd}}(q_v - q_{\text{vs}})q_c + C_{\text{cn}}(q_v - q_{\text{vs}})^+ q_{\text{cn}}, \tag{25}$$

$$S_{\text{ev}} = C_{\text{ev}}\frac{p}{\rho}(q_{\text{vs}} - q_v)^+ q_r, \tag{26}$$

$$S_{\text{cr}} = C_{\text{cr}} q_c q_r, \tag{27}$$

$$S_{\text{ac}} = C_{\text{ac}}(q_c - q_{\text{ac}})^+, \tag{28}$$

where $y^+ \equiv \max(0, y)$. Here $(C_{\text{cd}}, C_{\text{ev}}, C_{\text{cr}}, C_{\text{ac}}, C_{\text{cn}})$ are rate constants, q_{cn} quantifies the presence of condensation nuclei, and q_{ac} is a threshold for cloud water mixing ratio beyond which autoconversion of cloud water into precipitation becomes active. Note that for cloudless air ($q_c = 0$) we have positive condensation on cloud nuclei in oversaturated areas, whereas the inverse evaporation is suppressed in undersaturated air. However, as we shall see below, the condensation term will be defined implicitly from the asymptotics through the equation of water vapor at saturation, which also corresponds to a common definition of the condensation source term in the literature, see, for example, also [6,23].

The saturation threshold is given by the saturation vapor mixing ratio

$$q_{\text{vs}} = \frac{\rho_{\text{vs}}}{\rho_d}, \tag{29}$$

which can be expressed in terms of the saturation vapor pressure e_s through

$$q_{\text{vs}}(T, p) = \frac{E e_s(T)}{p - e_s(T)}, \qquad \text{where} \quad E = \frac{R_d}{R_v}. \tag{30}$$

The saturation pressure follows the Clausius–Clapeyron relation, [3,5],

$$\frac{\mathrm{d}\ln e_s}{\mathrm{d}T} = \frac{L_{\mathrm{ref}}\phi(T)}{R_v T^2}. \tag{31}$$

We do not take into account different temperatures for the liquid water, but note that the temperature of very large droplets with a diameter of ∼1 cm might differ from the ones of the surrounding air, which, however, are very rare. For a further discussion on the incorporation of a different temperature for liquid water droplets into the dynamics we refer to [21].

3 Non-dimensionalization and asymptotic scalings

3.1 Dimensionless characteristic quantities

Standard thermodynamic reference values for the tropics are

$$p_{\mathrm{ref}} = 10^5\ \mathrm{Pa}\,, \qquad T_{\mathrm{ref}} = 300\ \mathrm{K}\,, \qquad \rho_{\mathrm{ref}} = \frac{p_{\mathrm{ref}}}{R_d T_{\mathrm{ref}}} \approx 1.2\ \mathrm{kg/m^3}. \tag{32}$$

To address deep convection phenomena it should be appropriate to use the "bulk convective scales" for space and time, *i.e.*, the pressure scale height for horizontal and vertical length scales and the associated advection time scale based on a typical wind speed u_{ref},

$$\ell_{\mathrm{ref}} = h_{\mathrm{sc}} = \frac{p_{\mathrm{ref}}}{g\rho_{\mathrm{ref}}} \approx 8.8\,\mathrm{km}\,, \quad u_{\mathrm{ref}} \approx 10\ \mathrm{m/s}\,, \quad t_{\mathrm{ref}} = \frac{\ell_{\mathrm{ref}}}{u_{\mathrm{ref}}} \approx 15\ \mathrm{min}, \tag{33}$$

where the gravitational acceleration is $g = 9.8\ \mathrm{m/s^2}$. A reference flow velocity of about 10 m/s reasonably matches with both horizontal flow velocities in the tropics and updraft velocities in convective towers, although the latter can be larger in regions of large CAPE. The present analysis may not cover cases of CAPE much larger than, say, $1\,000\ \mathrm{m^2/s^2}$. See also the discussion toward the end of Sect. 4.1 below.

Based on these reference quantities the principal fluid dynamical parameters, *i.e.*, the Mach, barotropic Froude, and bulk convective scale Rossby numbers, are

$$\mathrm{M} = \frac{u_{\mathrm{ref}}}{\sqrt{p_{\mathrm{ref}}/\rho_{\mathrm{ref}}}} = \mathrm{Fr} = \frac{u_{\mathrm{ref}}}{\sqrt{g h_{\mathrm{sc}}}} \approx \frac{1}{30}, \qquad \mathrm{Ro}_B = \frac{u_{\mathrm{ref}}}{|2\boldsymbol{\Omega}_{\parallel}| h_{\mathrm{sc}}} \approx 10. \tag{34}$$

The thermodynamics of moist air is characterized by several further dimensionless quantities. At the standard temperature of $T_0 = 273.15$ K the specific heat capacities and gas constants and the latent heat of condensation amount to the values given in Table 1. The heat capacities vary slightly with temperature, but these variations are small enough to not affect the expansions carried out below, and they are therefore neglected in the following. The temperature dependence of the latent heat is considerable, however, and it has been accounted for already in (24). Using the latter, we see that the reference value $L_{\mathrm{ref}} = L(T_{\mathrm{ref}})$ for the tropical reference value $T_{\mathrm{ref}} = 300$ K only deviates slightly with $L_{\mathrm{ref}} \approx 2.4 \times 10^6$ J/kg. The reference value $L_{\mathrm{ref}}/(c_{\mathrm{pd}} T_{\mathrm{ref}})$ then reduces to approximately 8.1, such that the stated orders of magnitudes in Table 2 remain unchanged even for the tropical conditions. The listed parameters give rise to five independent dimensionless characteristic ratios and some more derived quantities as listed in Table 2.

The mixing ratios of the water constitutents are dimensionless by definition, and their typical magnitude in the atmosphere is set by the saturation water vapor mixing ratio at reference conditions,

$$q_{\mathrm{vs,ref}} = q_{\mathrm{vs}}(p_{\mathrm{ref}}, T_{\mathrm{ref}}) \approx 0.023, \tag{35}$$

see also [24].

3.2 Distinguished asymptotic limits

As explained, for example, in [8], asymptotic analysis in the presence of multiple small parameters generally requires the introduction of distinguished limits to uniquely identify one of many possible asymptotic limit regimes. The cited review introduced a particular distinguished limit for atmospheric modeling that couples the Mach, Froude, and Rossby numbers, and that has turned out to be rather uniformly useful across many different applications of scale analysis and asymptotics for the atmosphere. Specifically, this limit amounts to letting

$$\mathrm{M} = \mathrm{Fr} = \mathcal{O}\left(\varepsilon^{\frac{3}{2}}\right), \qquad \mathrm{Fr}_{\mathrm{int}} = \mathcal{O}\left(\varepsilon\right), \qquad \mathrm{Ro}_{\mathrm{B}} = \mathcal{O}\left(\varepsilon^{-1}\right), \tag{36}$$

where $\mathrm{Fr}_{\mathrm{int}} = u_{\mathrm{ref}}/c_{\mathrm{int}}$ is the Froude number based on a typical internal wave speed $c_{\mathrm{int}} = \sqrt{g h_{\mathrm{sc}}}\sqrt{\Delta\theta/T_{\mathrm{ref}}}$. Since, therefore, $\mathrm{Fr}_{\mathrm{int}} = \mathrm{Fr}/\sqrt{\Delta\theta/T_{\mathrm{ref}}}$, this leads to

$$\frac{\Delta\theta}{T_{\mathrm{ref}}} = \mathcal{O}\left(\varepsilon\right), \tag{37}$$

where $\Delta\theta \approx 30\ldots40$ K measures the increase in potential temperature across the height of the troposphere. This sets a realistic magnitude of ε to

$$\varepsilon \sim 1/10. \tag{38}$$

In the present paper, this distinguished limit for the dynamically relevant parameters will be tied in with two alternative scaling regimes characterizing the moist thermodynamics of air. As in [1] we use (35) and (38) to let

$$q_{\mathrm{vs,ref}} = \mathcal{O}\left(\varepsilon^2\right). \tag{39}$$

In agreement with the common assessment that the stratification of the near-equatorial troposphere is close to moist adiabatic, we identify the potential temperature difference $\Delta\theta$ with the typical temperature change associated with the total latent heat of condensation at saturation, *i.e.*, $\Delta\theta \sim q_{\mathrm{vs}} L/c_{\mathrm{pd}}$. Then, with (37) and (39) and evaluating at reference conditions we have

$$\frac{\Delta\theta}{T_{\mathrm{ref}}} = q_{\mathrm{vs,ref}}\frac{L_{\mathrm{ref}}}{c_{\mathrm{pd}}T_{\mathrm{ref}}} \quad i.e. \quad \frac{L_{\mathrm{ref}}}{c_{\mathrm{pd}}T_{\mathrm{ref}}} = \frac{L}{\varepsilon} \quad \text{with} \quad L = \mathcal{O}\left(1\right) \quad (\varepsilon \to 0). \tag{40}$$

As in [1] we adopt the Newtonian limit for dry air, *i.e.*,

$$\frac{R_d}{c_{\mathrm{pd}}} = \frac{\gamma - 1}{\gamma} = \varepsilon\Gamma. \tag{41}$$

Two alternative suggestions for coupled limit relations for the remaining characteristics of the moist thermodynamics of air are summarized in Table 2. The scaling labeled $\alpha = 1$ in the rightmost column pragmatically focuses on the bare magnitude of the dimensionless ratios and assigns the respective asymptotic scalings accordingly. Consistently, numbers in the range $0.4\ldots3.0$ are considered of order $\mathcal{O}\left(1\right)$, whereas numbers that are substantially larger or smaller are assumed to scale with appropriate powers of ε. While these assignments are consistent with the given magnitudes for the moist air parameters, they have the caveat of not representing a realizable limit for a mixture of gases: Obviously, we obtain two expressions for, say, the ratio R_d/R_v, namely $E = \mathcal{O}\left(1\right)$ and $(R_d/c_{\mathrm{pd}})(c_{\mathrm{pd}}/R_v) = \varepsilon\Gamma A = \mathcal{O}\left(\varepsilon\right)$ as $\varepsilon \to 0$. Although awkward at first, this may not pose a major difficulty. The thermodynamics of moist air may just be asymptotically compatible with a family of equation systems that features the same functional forms in the constitutive equations, but whose set of the determining parameters is less constrained. The results of Sect. 4.2 below corroborate this point of view.

In contrast, the scaling labeled $\alpha = 0$ appears to violate some basic order-of-magnitude estimates. Yet, this regime *is* consistent with the thermodynamics of a mixture of gases in the sense of similarity theory, and each of its scalings as given in Table 2 is argued for in Sect. 4.1 based on an analysis of the moist adiabatic hydrostatic state.

Although the Coriolis force does not play a dominant role in the present flow regime, it, nevertheless, appears in the hot tower asymptotics below. At latitude φ, we decompose the earth rotation vector into vertical and horizontal components,

$$2\boldsymbol{\Omega} = 2\left(\boldsymbol{\Omega}_{\perp} + \boldsymbol{\Omega}_{\parallel}\right) = 2\Omega\sin(\varphi)\boldsymbol{k} + 2\Omega\cos(\varphi)\boldsymbol{e}_N \tag{42}$$

where $\Omega = |\boldsymbol{\Omega}|$. Over the small scales considered here, the latitude varies by $\mathcal{O}\left(\varepsilon^3\right)$ (see [8]), so that we can work with a constant reference latitude φ_0. Interested in near-equatorial flows, we consider $\varphi_0 = \mathcal{O}(\varepsilon)$. This yields estimates for the Rossby numbers associated with the horizontal and vertical components of $\boldsymbol{\Omega}$,

$$\frac{2\boldsymbol{\Omega} h_{\mathrm{sc}}}{u_{\mathrm{ref}}} = \varepsilon^2 f\boldsymbol{k} + \varepsilon f_\perp \boldsymbol{e}_N + o\left(\varepsilon^2\right) \tag{43}$$

where

$$f = \frac{\sin(\varphi_0)}{\varepsilon^2 \mathrm{Ro}_B} = \mathcal{O}(1)\,, \qquad f_\perp = \frac{\cos(\varphi_0)}{\varepsilon \mathrm{Ro}_B} = \mathcal{O}(1) \tag{44}$$

are the effective Coriolis parameters. With these approximations and in our dimensionless notation, the Coriolis term reduces to

$$\frac{h_{\mathrm{sc}}}{u_{\mathrm{ref}}} 2 \times \mathbf{v} = \begin{pmatrix} -\varepsilon^2 f v + \varepsilon f_\perp w \\ \varepsilon^2 f u \\ -\varepsilon f_\perp u \end{pmatrix} = \varepsilon \begin{pmatrix} f_\perp w \\ 0 \\ -f_\perp u \end{pmatrix} + O(\varepsilon^2). \tag{45}$$

Typically the vertical Coriolis parameter $f_\perp$ is neglected, but the term $\varepsilon f_\perp w$ in the horizontal momentum equation does contribute to the dynamics when the horizontal velocities in the cloud tower are $\mathcal{O}(\varepsilon)$ and the characteristic time scale is that of advection in the vertical updraft (see [25] and the detailed analysis below).

3.3 Asymptotically rescaled governing equations

After non-dimensionalization, introduction of the coupled limits explained in the previous section, and switching between the two alternative scalings from Table 2, the governing equations read

$$\partial_t \rho_d + \nabla \cdot (\rho_d \boldsymbol{v}) = 0 \tag{46}$$

$$D_t \boldsymbol{u} + \varepsilon \boldsymbol{F}_\parallel + \frac{1}{\varepsilon^3}\frac{1}{\rho}\nabla_\parallel p = \varepsilon^2 \frac{\rho_d}{\rho} q_r V_r \partial_z \boldsymbol{u} \tag{47}$$

$$D_t w + \varepsilon \boldsymbol{F}_\perp + \frac{1}{\varepsilon^3}\frac{1}{\rho}\partial_z p = -\frac{1}{\varepsilon^3} + \varepsilon^2 \frac{\rho_d}{\rho} q_r V_r \partial_z w \tag{48}$$

$$C_\varepsilon D_t \ln\theta + \varepsilon^2 \Sigma_\varepsilon D_t \ln p + \varepsilon \frac{L\phi_\varepsilon}{T} D_t q_v = \varepsilon k_l q_r V_r \left(\partial_z \ln\theta + \varepsilon \Gamma \partial_z \ln p\right) \tag{49}$$

$$D_t q_v = S_{\mathrm{ev}} - S_{\mathrm{cd}} \tag{50}$$

$$D_t q_c = -\frac{1}{\varepsilon} S_{\mathrm{cr}} + S_{\mathrm{cd}} - S_{\mathrm{ac}} \tag{51}$$

$$D_t q_r - \frac{1}{\rho_d}\partial_z(\rho_d q_r V_r) = \frac{1}{\varepsilon} S_{\mathrm{cr}} + S_{\mathrm{ac}} - S_{\mathrm{ev}} \tag{52}$$

where

$$\rho = \rho_d \left(1 + \varepsilon^2 \left[q_v + q_c + q_r\right]\right) \tag{53}$$

$$p = \rho_d T (1 + \varepsilon^{1+\alpha} q_v / E) \tag{54}$$

$$T = \theta\, p^{\varepsilon\Gamma} \equiv \theta\, \pi \tag{55}$$

$$\boldsymbol{v} = \boldsymbol{u} + w\boldsymbol{k} \tag{56}$$

$$C_\varepsilon = 1 + \varepsilon\left[\varepsilon^\alpha k_v q_v + k_l (q_c + q_r)\right] \tag{57}$$

$$\Sigma_\varepsilon = \Gamma k_l (q_c + q_r) + \varepsilon^\alpha \kappa_v q_v \tag{58}$$

$$\phi_\varepsilon = 1 - \chi(T - 1)\,, \qquad \left(\chi = \frac{k_l - \varepsilon^\alpha k_v}{L}\right) \tag{59}$$

Here we neglected the turbulent and molecular transport terms, whose incorporation is left for future work, and we have introduced the Exner pressure π in (55). Since the *horizontal* momentum balance will only be expanded to first order, the additional horizontal momentum contributions due to water loading will not play

a role in the leading order dynamics. This is in line with the common assumption that their contributions are of lesser importance [3].

As in [1] we let

$$S_{\mathrm{cd}} = \frac{1}{\varepsilon^n}(C_{\mathrm{cd}}(q_v - q_{\mathrm{vs}})q_c + C_{\mathrm{cn}}(q_v - q_{\mathrm{vs}})^+ q_{\mathrm{cn}}), \tag{60}$$

$$S_{\mathrm{ev}} = C_{\mathrm{ev}}\frac{p}{\rho}(q_{\mathrm{vs}} - q_v)^+ q_r, \tag{61}$$

$$S_{\mathrm{cr}} = C_{\mathrm{cr}} q_c q_r, \tag{62}$$

$$S_{\mathrm{ac}} = C_{\mathrm{ac}}(q_c - \varepsilon q_{\mathrm{ac}})^+, \tag{63}$$

where now all appearing rate constants are $O(1)$. As already mentioned above, the condensation term will be obtained from (50) at saturated conditions leading to $S_{\mathrm{cd}} \approx -w\frac{\mathrm{d}q_{\mathrm{vs}}}{\mathrm{d}z}$. Depending on the scaling regime considered, the saturation mixing ratio is given as a function of pressure and temperature by

$$q_{\mathrm{vs}}(p, T) = \frac{E e_s(T)}{p - \varepsilon^{1+\alpha} e_s(T)}, \tag{64}$$

and the asymptotically rescaled Clausius–Clapeyron equation for the saturation vapor pressure, e_s, reads

$$\frac{\mathrm{d}\ln e_s}{\mathrm{d}T} = \frac{LA}{\varepsilon}\frac{\phi_\varepsilon(T)}{T^2} \tag{65}$$

with $\phi_\varepsilon(T)$ from (59).

4 The moist adiabat and the asymptotic scalings for the moisture parameters

The present section justifies the rationale behind the distinguished limit for the moisture quantities labeled $\alpha = 0$ in Table 2 by showing that the resulting moist adiabatic stratification is compatible with the general asymptotics framework from [8] as desired. This regime also turns out to be a "rich limit" in that it retains a maximal number of terms in the equations governing the moist adiabat among a broader family of possible scalings.

The leading and first-order asymptotic solutions for the moist adiabat are obtained for both scaling regimes from Table 2. Both turn out to compare favorably with a high-accuracy numerical solution based on the unapproximated equations.

4.1 Consequences of different scaling limits for the moist adiabat

The embedding of moist thermodynamics into the asymptotic modeling framework requires a careful balance of various large and small quantities. This is to be achieved through the appropriate choice of a distinguished limit tying these various quantities to one small reference parameter, $\varepsilon \ll 1$. To investigate the consequences which different choices of distinguished limits would imply, we consider the following rather general scaling scheme

$$\frac{L_{\mathrm{ref}}}{c_{\mathrm{pd}}T_{\mathrm{ref}}} = \frac{L}{\varepsilon^a}, \quad \frac{R_d}{c_{\mathrm{pd}}} = \varepsilon^b \Gamma, \quad \frac{R_v}{c_{\mathrm{pv}}} = \varepsilon^{b_v}\Gamma_v, \quad \frac{c_l}{c_{\mathrm{pd}}} = \frac{k_l}{\varepsilon^{b_l}}, \quad \frac{R_d}{R_v} = \varepsilon^c E. \tag{66}$$

Here L, Γ, Γ_v, and E are $\mathcal{O}(1)$ as $\varepsilon \to 0$ and the (positive) exponents a, b, b_v, b_l, c are not further specified as yet. For a scaling regime appropriate for atmospheric applications, and consistent with the developments of the previous section, we will discuss the consequences of choosing $a = b = 1$, and $b_v, b_l, c \in \{0, 1\}$ below. For the scaling of the r.h.s. of the Clausius–Clapeyron relation in (31) the choices in (66) imply

$$\frac{L_{\mathrm{ref}}}{R_v T_{\mathrm{ref}}} = \frac{1}{\varepsilon^{a+b-c}}\frac{LE}{\Gamma} \equiv \frac{AL}{\varepsilon^d} \qquad \text{where} \qquad d = a + b - c. \tag{67}$$

Also we account for the generally small values of the saturation water vapor mixing ratio q_{vs} and pressure e_s by letting their bare values before division by the reference value from (35) satisfy the scaling

$$\widehat{q}_{\mathrm{vs}} = \varepsilon^e \, q_{\mathrm{vs}} \,, \qquad \widehat{e}_s = \varepsilon^{e-c} \, e_s, \tag{68}$$

with $q_{\mathrm{vs}}, e_s = \mathcal{O}(1)$ as $\varepsilon \to 0$. This is motivated by the constitutive relation between the saturation mixing ratio $\widehat{q}_{\mathrm{vs}}$ and the saturation water vapor pressure $\widehat{e}_s$,

$$\varepsilon^e q_{\mathrm{vs}} = \widehat{q}_{\mathrm{vs}} = \frac{R_d}{R_v} \frac{\widehat{e}_s}{p - \widehat{e}_s} = \frac{\varepsilon^e E e_s}{p - \varepsilon^{e-c} e_s}, \tag{69}$$

where we used the last entry of (66).

The equations governing the moist adiabatic stratification consist of the potential temperature evolution equation (49) specialized to a vertical column neglecting the dissipative source and sedimentation of rain terms and requiring exact balance of all vertical advection terms, and the vertical momentum equation (48) specialized to hydrostatic balance. With the scalings introduced above, and using the definition of the Exner pressure π in (55), these equations become

$$\frac{\mathrm{d} \ln \theta}{\mathrm{d}z} = -\varepsilon^{e-a} \frac{L \phi_\varepsilon(T)}{C_\varepsilon \pi \theta} \frac{\mathrm{d}}{\mathrm{d}z} q_{\mathrm{vs}}(\theta, \pi; \varepsilon) - \varepsilon^{e-b} \frac{\Sigma_\varepsilon}{C_\varepsilon} \frac{1}{\Gamma} \frac{\mathrm{d} \ln \pi}{\mathrm{d}z} \tag{70}$$

$$\frac{\mathrm{d} \ln \pi}{\mathrm{d}z} = -\varepsilon^b \frac{\Gamma}{\pi \theta} \frac{1 + \varepsilon^e q_{\mathrm{vs}}}{1 + \varepsilon^{e-c} q_{\mathrm{vs}} / E} \tag{71}$$

For the saturation water vapor mixing ratio, q_{vs}, the dependence on the unknowns θ, π follows from the definition of e_s in (69) which depends on temperature only so that, with $T = \pi\theta$,

$$q_{\mathrm{vs}}(\theta, \pi; \varepsilon) = \frac{E e_s(\theta\pi; \varepsilon)}{\pi^{1/\varepsilon^b \Gamma} - \varepsilon^{e-c} e_s(\theta\pi; \varepsilon)}, \tag{72}$$

where the Clausius–Clapeyron relation for e_s reads as

$$\frac{1}{e_s} \frac{\mathrm{d}e_s}{\mathrm{d}T} = \frac{1}{\varepsilon^d} \frac{AL}{T^2} \phi_\varepsilon(T) \tag{73}$$

with

$$\phi_\varepsilon(T) = 1 + \chi_\varepsilon (T - 1) \qquad \text{where} \qquad \chi_\varepsilon = \varepsilon^{a-b_l} \frac{k_l}{L} - \varepsilon^{a+b-b_v-c} \frac{k_v}{L} \tag{74}$$

and $\varepsilon^{b-b_v-c} k_v = c_{\mathrm{pv}}/c_{\mathrm{pd}} = (R_d/c_{\mathrm{pd}})(R_v/R_d)(c_{\mathrm{pv}}/R_v) = \varepsilon^{b-b_v-c} \Gamma/(E\Gamma_v)$.

The scalings and governing equations for the moist adiabatic stratification summarized in (66)–(74) are combined in "Appendix A" to eliminate the derivative $\mathrm{d}q_{\mathrm{vs}}/\mathrm{d}z$ from (70), and this yields a scaled effective equation for the potential temperature. Keeping all dominant contributions for $\varepsilon \to 0$ (see "Appendix A.1" for what "dominant" refers to precisely), this equation reads

$$\frac{\mathrm{d}\theta}{\mathrm{d}z} = \varepsilon^b \frac{\Gamma}{\pi} \left(1 - \varepsilon^{a+d-e} \frac{I_\varepsilon + \varepsilon^{e-a-b} \frac{L\phi_\varepsilon}{\Gamma T} q_{\mathrm{vs}}}{\frac{AL^2 \phi_\varepsilon^2}{T^2} q_{\mathrm{vs}} + \varepsilon^{a+d-e} I_\varepsilon} \right), \tag{75}$$

where $I_\varepsilon = 1 - \varepsilon^{e-c} e_s / p$. To obtain a θ-variation that is small of order $\mathcal{O}\left(\varepsilon^b\right)$ as desired here, we must require $a + d - e \geq 0$, assuming for the moment that the remaining powers of ε in (158) have positive exponents. This will be verified below in hindsight. When $a + d - e > 0$, (158) combined with the equation for the Exner pressure from (71) yields

$$\frac{\mathrm{d}\theta}{\mathrm{d}z} = \varepsilon^b \frac{\Gamma}{\pi} (1 + o(1)) \qquad \frac{\mathrm{d}\pi}{\mathrm{d}z} = -\varepsilon^b \frac{\Gamma}{\theta} \qquad \text{and hence} \qquad \frac{\mathrm{d}T}{\mathrm{d}z} = \frac{\mathrm{d}\theta\pi}{\mathrm{d}z} = o\left(\varepsilon^b\right), \tag{76}$$

i.e., one finds temperatures with lesser variation across the troposphere than that of the potential temperature, which is not realistic.

In contrast, when $a + d - e = 0$, the second term in the bracket in (158) is of order unity and there will be vertical variations of the background temperature to order ε^b, comparable to those of π and θ. Thus, using (67), we let

$$e = a + d = 2a + b - c. \tag{77}$$

Consistency with the unified asymptotic modeling framework summarized in [8] requires potential temperature stratifications of order $\mathcal{O}(\varepsilon)$, *i.e.*, we let $b = 1$. Considering that $L_{\mathrm{ref}}/c_{\mathrm{pd}}T_{\mathrm{ref}} \approx 9.1$ as shown in Table 2, and with $\varepsilon \sim 1/10$, the most reasonable choice for a in (66) is $a = 1$ as well. Going back to (75) we observe that the second term in the numerator on the r.h.s. will be negligible asymptotically if $e > a + b$, while we obtain a classical "rich limit" that maintains all effects covered by (75) simultaneously if we let $e = a + b = 2$. This corresponds to $q_{\mathrm{vs}} = \mathcal{O}(\varepsilon^2)$ in line with the earlier order of magnitude assessment in (39). With this rich limit adopted, (77) implies $c = 1$. To summarize, we let

$$a = b = c = 1 \qquad \text{and} \qquad e = 2. \tag{78}$$

Admittedly, letting $c = 1$, *i.e.*, $R_d/R_v \approx 0.62 = \varepsilon E$ may appear a bit extreme, and $c = 0$ seems more reasonable. Yet, this would imply $e = 3$ following the arguments given above, *i.e.*, it would imply that the mixing ratios of the water constituents are $\mathcal{O}(\varepsilon^3)$. This, in turn, is not satisfactory either: First, the mixing ratios of the water constituents have a typical magnitude of 1%, and this matches with $\mathcal{O}(\varepsilon^2)$ much better than with $\mathcal{O}(\varepsilon^3)$ (see Fig. 1 below). Secondly, the buoyancy effects of water loading are generally thought to be important, and this leads us to an estimate of their contribution to CAPE. Integrated across the troposphere, water loadings of order $1\% \sim \varepsilon^2$ amount to potential energies of order $10^{-2} \cdot g h_{\mathrm{sc}} \sim 10^3\ \mathrm{m}^2/\mathrm{s}^2$. This is a realistic level of CAPE in many situations, and one would aim for a scaling of the water constitutent mixing ratios that allows for their buoyancy effects to participate in the related dynamics. With $q \sim \mathcal{O}(\varepsilon^3)$, however, the influence of water loading-induced buoyancy would be restricted to rather tame situations with CAPE merely of order $10^2\ \mathrm{m}^2/\mathrm{s}^2$.

Notably, the choice of b_v, *i.e.*, whether or not we assume a Newtonian limit for the water vapor, does not play a role up to this point. The last entry in the column for $\alpha = 0$ in Table 1 provides a guideline, however. Under the adopted scaling, $R_v/c_{\mathrm{pd}} = \mathcal{O}(1)$ and it has an actual value for moist air of 0.46. At the same time, the Newtonian limit for dry air implies $R_d/c_{\mathrm{pd}} = \mathcal{O}(\varepsilon)$. Thus, the combination $\frac{c_{\mathrm{pv}}}{c_{\mathrm{pd}}}\frac{R_d}{c_{\mathrm{pd}}} - \frac{R_v}{c_{\mathrm{pd}}}$ is asymptotically equal to $-R_v/c_{\mathrm{pd}}$, and hence negative, for $b_v < 1$, while it is asymptotically large for $b_v > b$. Only $b = b_v = 1$ will allow for the adjustment to a finite positive value in the limit, and this is why we adopt the Newtonian limit for water vapor as well with $R_v/c_{\mathrm{pv}} = \varepsilon\Gamma_v$.

Given that $b_v = 1$, the exponent b_l, which scales the liquid water heat capacity in (66), should be larger or equal to unity, as the liquid water heat capacity exceeds that of water vapor by a factor larger than two. It is not reasonable, on the other hand, to let $b_l > 1$, because this would imply that the temperature dependence of the latent heat would dominate relative to its reference value, see (74), and this is not realistic: The temperature-induced relative variation of latent heat across the troposphere amounts to only 5%. Thus, we chose $b_l = 1$ as well, and this completes the discussion of the scaling for $\alpha = 0$ from Table 2.

4.2 Asymptotic analysis versus numerical computation of the moist adiabat

Here we compare high-accuracy numerical solutions for the moist adiabatic hydrostatic state, described in detail by (70) and (71), with leading and first-order asymptotic solutions under the two scaling regimes from Table 2.

The full, somewhat lengthy, detail of the asymptotic analysis is given in "Appendix B." Here we just summarize the leading order analysis to provide an impression of how the calculations proceed. Keeping only the dominant terms in the equations so as to streamline the exposition for this chapter, we have

$$\frac{\mathrm{d}\theta}{\mathrm{d}z} = -\varepsilon\frac{L}{\pi}\frac{\mathrm{d}q_{\mathrm{vs}}}{\mathrm{d}z} \tag{79}$$

$$\frac{\mathrm{d}\pi}{\mathrm{d}z} = -\varepsilon\frac{\Gamma}{\theta} \tag{80}$$

together with the constitutive relations

$$q_{\rm vs} = \frac{E e_s(T)}{p}\,, \qquad p = \pi^{1/\varepsilon\Gamma}\,, \qquad T = \pi\theta\,, \qquad \frac{1}{e_s}\frac{\mathrm{d}e_s}{\mathrm{d}T} = \frac{1}{\varepsilon}\frac{AL}{T^2}. \tag{81}$$

The unknowns θ, π are expanded as

$$\begin{aligned} \theta &= 1 + \varepsilon\theta^{(1)}(z) + o(\varepsilon) \\ \pi &= 1 + \varepsilon\pi^{(1)}(z) + o(\varepsilon) \end{aligned}. \tag{82}$$

Inserting the expansion of θ into (80) we obtain

$$\pi^{(1)}(z) = -\Gamma z, \tag{83}$$

and then the constitutive equations for pressure and temperature in (82) yield

$$T = 1 + \varepsilon T^{(1)} + o(\varepsilon)\,, \qquad T^{(1)}(z) = \theta^{(1)}(z) - \Gamma z \tag{84}$$

$$p = p^{(0)} + \varepsilon p^{(1)} + o(\varepsilon)\,, \qquad p^{(0)}(z) = \lim_{\varepsilon\to 0}(1 - \varepsilon\Gamma z)^{\frac{1}{\varepsilon\Gamma}} = e^{-z}. \tag{85}$$

Next we observe that $q_{\rm vs}$ is given as a function of temperature and pressure, $(T,\, p)$, and these are functions of our primary unknowns θ, π in turn. After a short calculation applying the chain rule appropriately, we have

$$\frac{\mathrm{d}q_{\rm vs}}{\mathrm{d}z} = q_{\rm vs}\left(\frac{\mathrm{d}\ln e_s}{\mathrm{d}T}\left[\pi\frac{\partial\theta}{\mathrm{d}z} + \theta\frac{\partial\pi}{\mathrm{d}z}\right] - \frac{\mathrm{d}\ln p}{d\pi}\frac{\mathrm{d}\pi}{\mathrm{d}z}\right) \tag{86}$$

$$= q_{\rm vs}\left(\frac{AL}{T^2}\left[-L\frac{\mathrm{d}q_{\rm vs}}{\mathrm{d}z} - \Gamma\right] + \frac{1}{\theta\pi}\right). \tag{87}$$

Using the asymptotic ansatz for θ, π, T, p, keeping only the leading terms, and solving for $(\mathrm{d}q_{\rm vs}^{(0)}/\mathrm{d}z)^{-1}$,

$$\frac{\mathrm{d}z}{\mathrm{d}q_{\rm vs}^{(0)}} = -\frac{1}{AL\Gamma - 1}\left(AL^2 + \frac{1}{q_{\rm vs}^{(0)}}\right). \tag{88}$$

This is readily solved by

$$\ln\left(\frac{q_{\rm vs}^{(0)}(z)}{q_{\rm vs}^{(0)}{}_0}\right) + AL^2\left(q_{\rm vs}^{(0)}(z) - q_{\rm vs}^{(0)}{}_0\right) = -(AL\Gamma - 1)\,z. \tag{89}$$

Returning to (79) and keeping again only the leading order terms we find

$$\theta^{(1)}(z) = -L\left(q_{\rm vs}^{(0)}(z) - q_{\rm vs}^{(0)}{}_0\right) + \theta_0^{(1)}\,, \tag{90}$$

for the first-order potential temperature. Here $\theta_0^{(1)} \equiv \theta^{(1)}(0)$ captures deviations of the near-surface temperature from the reference temperature used in the non-dimensionalization of the equations.

Equations (83), (89), and (90) describe the moist adiabatic profile asymptotically to leading order in ε. This leading order solution is shared by both scalings from Table 2. For comparison, numerical solutions of the full equations for the moist adiabat without asymptotic approximation were obtained using the MATLAB `ode23s()` routine. Variations of the error tolerance option of the routine in the range `tol` $= 10^{-4} \ldots 10^{-10}$ produced indistinguishable results at the level of the graphics output.

The thick solid lines in Fig. 1 represent the leading order asymptotic solutions for Exner pressure π (leftmost line), temperature $T = \theta\pi$ (line in the middle), and potential temperature θ (rightmost line). The open circles display the numerical solutions. There is good qualitative agreement, whereas quantitative accuracy leaves room for improvement.

To improve on this, we worked out the next order asymptotic corrections in "Appendix B" for both scaling regimes and the results are included in Fig. 1 as well. The thin solid lines represent the asymptotic solutions to leading and first order for the scaling labeled $\alpha = 0$, whereas the thin dash-dotted lines represent the same for $\alpha = 1$. Deviations of these approximations from the numerical results are in the range of a few percent so that good quantitative accuracy is now obtained as well.

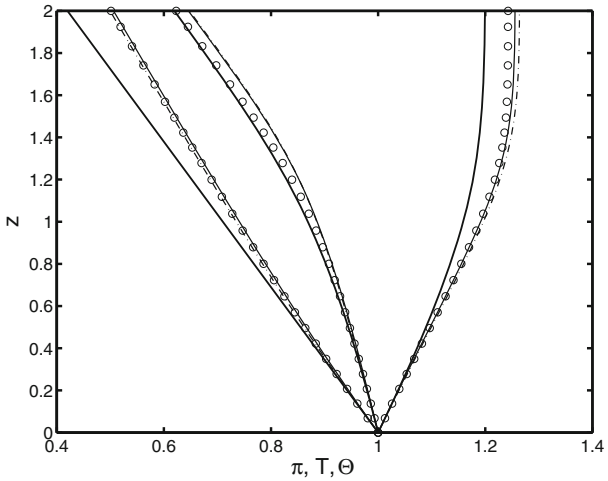

Fig. 1 Comparison of asymptotic and highly accurate numerical approximations to the hydrostatic moist adiabat. *Thick solid curves*: leading order asymptotics; *thin solid curve(s)*: first-order accurate asymptotics for the regime with $\alpha = 0$; *dash-dotted curves*: first-order accurate asymptotics for $\alpha = 1$; *circles*: error-controlled numerical solution of the full moist adiabatic equations (only every third data point used by the adaptive MATLAB routine `ode23s()` is displayed). Leftmost triple of distributions: Exner pressure π; middle triple: temperature T; right triple: potential temperature θ

Although one might expect even better accuracy formally, since $\varepsilon \sim 1/10$ and the leftover truncation errors are $\mathcal{O}\left(\varepsilon^3\right)$, we consider the results in Fig. 1 to be quite satisfactory for the following reason: The Newtonian approximation of the equation of state from (41) sets $(\gamma - 1)/\gamma = \varepsilon\Gamma$ as $\varepsilon \to 0$, while the given concrete model parameters produce a value of $(\gamma - 1)/\gamma = 0.29$, which is not a very small number. This places limits on the accuracy that can be expected from the lowest order asymptotic approximations.

5 Convective time scale dynamics of an upright cloud tower

In this section we adopt the scaling regime with $\alpha = 1$ from Table 2, discussing deviations between the two regimes briefly at the end in a separate subsection.

5.1 Cloud tower scaling

Here we study flows within a deep convective cloud tower with vertical extent comparable to the pressure scale height, $h_{\text{sc}} \sim 10$ km, but with narrow horizontal support of order $\varepsilon h_{\text{sc}} \sim 1$ km, see Fig. 2. We restrict to a single cloud tower embedded in a quiescent environment to focus just on the dynamics of convection within. To resolve the small horizontal scale we introduce the stretched coordinate

$$\boldsymbol{\eta} = \frac{\boldsymbol{x}}{\varepsilon}, \tag{91}$$

as sketched in Fig. 2, so that the solution ansatz to order $\mathcal{O}\left(\varepsilon^N\right)$ for any of the unknowns, ϕ, reads

$$\phi(t, \mathbf{x}, z; \varepsilon) = \sum_{i=0}^{N} \varepsilon^i \phi^{(i)}(t, \boldsymbol{\eta}, z) + o\left(\varepsilon^N\right), \tag{92}$$

$$\phi^{(i)}(t, \boldsymbol{\eta}, z) = \Phi_i(z) + \widetilde{\phi}^{(i)}(t, \boldsymbol{\eta}, z) \tag{93}$$

i.e., we split the perturbation functions into their purely z-dependent background contributions and their small-scale variations within the cloud tower.

We are interested in dominantly vertical updrafts with updraft velocities of order unity, *i.e.*, of order 10 m/s in dimensional terms, developing on the $\mathcal{O}(1)$ time scale, *i.e.*, on time scales of order $h_{\text{sc}}/u_{\text{ref}} \sim 20$ min in dimensional terms. We anticipate that this implies either a constant or vanishing background wind, i.e., only

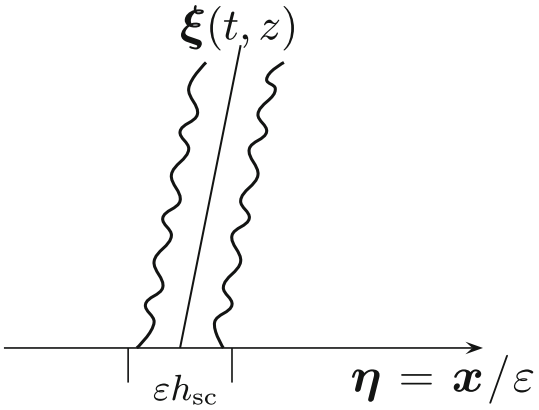

Fig. 2 Deep convective tower scaling

weak wind shear, and we assume, if necessary, a moving coordinate system within which the background state is stationary. In this frame of reference the horizontal velocity is expanded as

$$\boldsymbol{u} = \varepsilon \boldsymbol{u}^{(1)} + \varepsilon^2 \boldsymbol{u}^{(2)} + O(\varepsilon^3)\,, \tag{94}$$

whereas the vertical velocity component has a leading order contribution describing the intense up- and downdrafts of interest

$$w = w^{(0)} + \varepsilon w^{(1)} + O(\varepsilon^2). \tag{95}$$

5.2 Rescaled governing equations

The rescaled governing equations are obtained by replacing

$$\nabla_\parallel \to \frac{1}{\varepsilon}\nabla_{\boldsymbol{\eta}}\,, \tag{96}$$

leading, in particular, to the transport operator

$$D_t = \partial_t + \frac{1}{\varepsilon}\boldsymbol{u}\cdot\nabla_{\boldsymbol{\eta}} + w\partial_z. \tag{97}$$

Then, the scaled governing equations become

$$\partial_t \rho_d + \frac{1}{\varepsilon}\nabla_{\boldsymbol{\eta}}\cdot(\rho_d \boldsymbol{u}) + \partial_z(\rho_d w) = 0, \tag{98}$$

$$D_t \boldsymbol{u} + \varepsilon \mathbf{F}_\parallel = -\frac{1}{\varepsilon^4}\frac{1}{\rho}\nabla_{\boldsymbol{\eta}} p + \varepsilon^2 \frac{\rho_d}{\rho} q_r V_r \partial_z \boldsymbol{u}\,, \tag{99}$$

$$D_t w + \varepsilon \mathbf{F}_\perp = -\frac{1}{\varepsilon^3}\frac{1}{\rho}(\partial_z p + \rho) + \varepsilon^2 \frac{\rho_d}{\rho} q_r V_r \partial_z w\,, \tag{100}$$

$$\begin{aligned} C_\varepsilon D_t \ln\theta + \varepsilon^2 \Sigma_\varepsilon D_t \ln p \; &- \varepsilon k_l q_r V_r\,(\partial_z \ln\theta + \varepsilon \Gamma \partial_z \ln p) \\ &= \varepsilon \frac{L}{T}(1 - \chi(T-1))(S_{\rm cd} - S_{\rm ev}) \end{aligned} \tag{101}$$

with C_ε, Σ_ε from (57) and (58), respectively. Accordingly, we have

$$D_t q_v = S_{\rm ev} - S_{\rm cd}\,, \tag{102}$$

$$D_t q_c = S_{\rm cd} - \frac{S_{\rm cr}}{\varepsilon} - S_{\rm ac}\,, \tag{103}$$

$$D_t q_r - \frac{1}{\rho_d}\partial_z(\rho_d q_r V_r) = \frac{S_{\rm cr}}{\varepsilon} - S_{\rm ev} + S_{\rm ac}\,, \tag{104}$$

for the moisture dynamics, and we conclude from the horizontal momentum balance in (99) that the expansion of the thermodynamic quantities about the hydrostatic background remains valid at least up to $O(\varepsilon^2)$

$$\rho = \rho_h + O(\varepsilon^2)\,, \qquad p = p_h + O(\varepsilon^2). \tag{105}$$

5.3 Small-scale dynamics

5.3.1 Mass and momentum balances

The horizontal momentum balance yields

$$\nabla_{\boldsymbol{\eta}} \pi^{(j)} = 0 \qquad (j = 0, ..., 5) \tag{106}$$

$$D_t^{(0)} \boldsymbol{u}^{(1)} + f_\perp w^{(0)} \mathbf{e}_1 + \frac{1}{\Gamma} \nabla_{\boldsymbol{\eta}} \pi^{(6)} = 0, \tag{107}$$

where π is the Exner pressure defined in (55), and

$$D_t^{(0)} = \partial_t + \boldsymbol{u}^{(1)} \cdot \nabla_{\boldsymbol{\eta}} + w^{(0)} \partial_z\,, \qquad \mathbf{e}_1 = (1, 0)^T\,, \tag{108}$$

and $\pi^{(6)}$ satisfies the elliptic equation

$$\frac{1}{\Gamma} \Delta_{\boldsymbol{\eta}} \pi^{(6)} = -\nabla_{\boldsymbol{\eta}} \cdot \left(\partial_t \boldsymbol{u}^{(1)} + \boldsymbol{u}^{(1)} \cdot \nabla_{\boldsymbol{\eta}} \boldsymbol{u}^{(1)} + w^{(0)} \left(\partial_z \boldsymbol{u}^{(1)} + f_\perp \mathbf{e}_1 \right) \right). \tag{109}$$

An expression for $\nabla_{\boldsymbol{\eta}} \cdot \partial_t \boldsymbol{u}^{(1)} = \partial_t (\nabla_{\boldsymbol{\eta}} \cdot \boldsymbol{u}^{(1)})$ follows from the leading order mass conservation equation,

$$\partial_t \left(\nabla_{\boldsymbol{\eta}} \cdot \boldsymbol{u}^{(1)} \right) = (1 - \partial_z) \partial_t w^{(0)}. \tag{110}$$

where we use that pressure and density are dominated to leading order by $p^{(0)} = \rho^{(0)} = e^{-z}$ on account of (85), and $\rho = p/T(1 + \varepsilon^2(q_v + q_c + q_r))/(1 + \varepsilon^2 q_v/E)$, for the regime with $\alpha = 1$ from Table 2.

Anticipating the results to be derived in the subsequent sections, we note here that (109) is an elliptic equation for $\pi^{(6)}$ despite the appearance on the right-hand side of the time derivative of $\boldsymbol{u}^{(1)}$: Via (110) this time derivative is replaced with that of $w^{(0)}$, and for both the saturated and undersaturated regions we will derive equations that express $w^{(0)}$ as a function of the leading order rain water mixing ratio, $q_r^{(0)}$. The principal result of our analysis is closed evolution equations for the latter in both regimes, so the velocity time derivative in (109) can be calculated after the $q_r^{(0)}$ equations have been solved. Thus, $\pi^{(6)}$ plays the usual low Mach number limiting role of a Lagrange multiplier guaranteeing that $\boldsymbol{u}^{(1)}$ observes a divergence constraint.

Just as the pressure gradient alone dominates the horizontal momentum balance up to 6th order, see (106), the vertical momentum balance is dominated by the pressure gradient up to fourth order and the accompanying gravity terms. In particular, at second order, the vertical pressure gradient and the gravity term are in balance. Since, furthermore, the pressure is horizontally homogeneous at that order, we subtract the balance in the environment of the cloud tower from the balance of the terms within to find zero total buoyancy at that order,

$$\widetilde{\theta}^{(2)} = \theta^{(2)} - \overline{\theta}^{(2)} = -\left(\left(\frac{1}{E} - 1 \right) \left(q_v^{(0)} - \overline{q}_v^{(0)} \right) - q_c^{(0)} - q_r^{(0)} \right). \tag{111}$$

This balance will play a central role in what follows.

Physically speaking, the pressure is horizontally homogeneous at the relevant order for the same reason for which boundary layer theory works with pressures being imposed from the farfield and constant through the layer. The only difference is that here we have upright towers instead of the (usually) horizontal surface boundary layers. As a consequence, upon subtraction of the hydrostatic balance outside the tower from the hydrostatic relation valid inside, the vertical pressure gradient cancels, and only the deviations of buoyancy terms inside from those outside the tower remain. This is the essence of (111).

5.3.2 Saturated air

Within the cloud tower, the air is by definition saturated with moisture, such that the deviation of the leading order water vapor content satisfies

$$q_v^{(0)} = q_{\mathrm{vs}}^{(0)}(z). \tag{112}$$

The cloud water mixing ratio vanishes to leading order, *i.e.*,

$$q_c = \varepsilon q_c^{(1)} + O(\varepsilon^2) \tag{113}$$

due to rapid collection of cloud water by the falling rain in deep convective columns, see the term $-\varepsilon^{-1} S_{\mathrm{cr}}$ in (103) and [26] for corroboration. As a consequence, the term $-q_c^{(0)}$ in (111) vanishes identically. Also, the leading order source terms for cloud water must then balance in the equation for the cloud water mixing ratio, and this determines the first-order cloud water content as a function of $w^{(0)}$ and $q_r^{(0)}$ through

$$-w^{(0)} \frac{\mathrm{d}q_{\mathrm{vs}}^{(0)}}{\mathrm{d}z} = S_{\mathrm{cr}}^{(1)} = C_{\mathrm{cr}} q_c^{(1)} q_r^{(0)}. \tag{114}$$

Note that this relation also implies $w^{(0)} \geq 0$ in the saturated region since the mixing ratios must be positive: As a consequence, vertical upward motion is possible against the stable stratification as the latter is overcome by the release of latent heat. In contrast, downward motion with leading order velocities, *i.e.*, negative $w^{(0)}$, cannot occur. Overcoming the stable potential temperature stratification in that direction would require re-evaporation of liquid water at a sufficient rate. Re-evaporation of rain at such rates would require substantial undersaturation which is obviously not available in a saturated column. Re-evaporation of cloud water at such rates sustained over the convective time scale would require the presence of sufficient amounts of cloud water. Since, however, $q_c^{(0)} \equiv 0$, the cloud mixing ratio is $q_c = \mathcal{O}(\varepsilon)$, so that such downdrafts would stop after $\mathcal{O}(\varepsilon)$ time scales.

The total liquid water content is thus equivalent to the rain water content at leading order, and its mixture fraction obeys the transport equation

$$D_t^{(0)} q_r^{(0)} - \frac{1}{\rho^{(0)}} \partial_z \left(\rho^{(0)} q_r^{(0)} V_r \right) = S_{\mathrm{cr}}^{(1)} = -w^{(0)} \frac{\mathrm{d}q_{\mathrm{vs}}^{(0)}}{\mathrm{d}z}. \tag{115}$$

The buoyancy balance from (111), with $q_c^{(0)}$ eliminated and with $q_v^{(0)} = q_{\mathrm{vs}}^{(0)}$, $\overline{q}_v^{(0)}$ replaced with known functions of z, expresses the potential temperature perturbation as a function of $q_r^{(0)}$ only. At the same time, however, $\widetilde{\theta}^{(2)}$ must satisfy the second-order potential temperature transport equation,

$$D_t^{(0)} \widetilde{\theta}^{(2)} = w^{(0)} \frac{\mathrm{d}\Delta\Theta^{(2)}}{\mathrm{d}z} + q_r^{(0)} \left(V_r - w^{(0)} \right) k_l \frac{\mathrm{d}T^{(1)}}{\mathrm{d}z}, \tag{116}$$

where $\Delta\Theta^{(2)} = \Theta_{\mathrm{ad}}^{(2)} - \overline{\theta}^{(2)}$ is the difference between the second-order moist adiabatic and the second-order background potential temperature distributions. The determining equations for $\Theta_{\mathrm{ad}}^{(2)}(z)$ are worked out in "Appendix B.3."

The rain water mixing ratio, $q_r^{(0)}$, in turn satisfies (115), and combining these constraints yields an algebraic relation for the vertical velocity,

$$\begin{aligned} w^{(0)} \left(k_l q_r^{(0)} \frac{\mathrm{d}T^{(1)}}{\mathrm{d}z} - \frac{\mathrm{d}\Delta\Theta^{(2)}}{\mathrm{d}z} - \frac{1}{E} \frac{\mathrm{d}q_{\mathrm{vs}}^{(0)}}{\mathrm{d}z} + \left(\frac{1}{E} - 1 \right) \frac{\mathrm{d}\overline{q}_v^{(0)}}{\mathrm{d}z} \right) \\ = k_l q_r^{(0)} V_r \frac{\mathrm{d}T^{(1)}}{\mathrm{d}z} - \frac{1}{\rho_0} \partial_z \left(\rho_0 q_r^{(0)} V_r \right), \end{aligned} \tag{117}$$

where we recall that $T^{(1)} = \theta^{(1)} - \Gamma z$.

We note that if $q_r^{(0)} \equiv 0$, then the vertical velocity vanishes as well. This means that on this long time scale under consideration, sustaining a vertical velocity is only possible if the system produces precipitation and, in turn, where there is no vertical velocity, no rain water can be found.

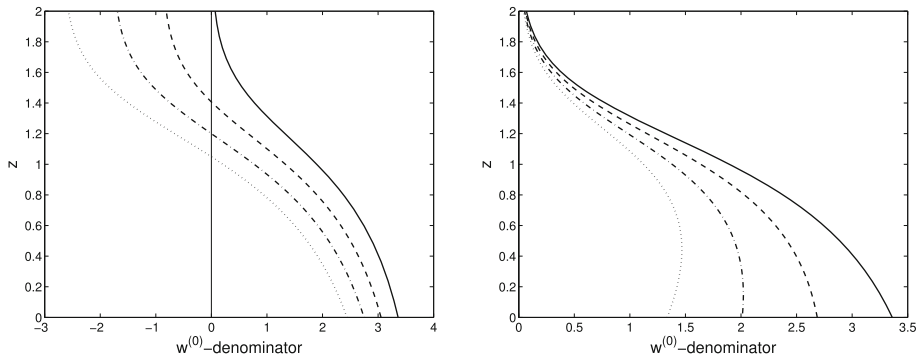

Fig. 3 The denominator in the determining equation (118) for vertical velocity in saturated air for $\Delta\Theta_2 = 0$ and $q_r^{(0)} = 2.2, 1.6, 0.8, 0.0$ (*dotted*, *dash-dotted*, *dashed*, and *solid curves*) (*left panel*), and for $q_r^{(0)} = (2.2, 1.6, 0.8, 0.0)\, q_{\mathrm{vs}}^{(0)}(z)$ (*right panel*)

A rewrite of $w^{(0)}$ according to (117) reveals the following dependence on $q_r^{(0)}$ and $\partial_z q_r^{(0)}$

$$w^{(0)} = V_r \frac{\left[k_l \frac{\mathrm{d}T^{(1)}}{\mathrm{d}z} + 1\right] q_r^{(0)} - \partial_z q_r^{(0)}}{k_l \frac{\mathrm{d}T^{(1)}}{\mathrm{d}z} q_r^{(0)} - \frac{\mathrm{d}\Delta\Theta^{(2)}}{\mathrm{d}z} - \frac{1}{E}\frac{\mathrm{d}q_{\mathrm{vs}}^{(0)}}{\mathrm{d}z} + \left(\frac{1}{E} - 1\right)\frac{\mathrm{d}\overline{q_v}^{(0)}}{\mathrm{d}z}}. \tag{118}$$

The denominator is rather benign for realistic values of $q_r^{(0)} \leq 2.4$ and for dimensionless heights less than 1.0, corresponding to a domain height of 10 km, as shown in Fig. 3, left panel. The right panel of Fig. 3 shows the denominator for the more realistic setting where the rain water mixing ratio scales with the local saturation water vapor mixing ratio. In this case, the denominator even stays positive throughout the bottom two scale heights of the atmosphere.

As a consequence, the qualitative properties of the q_r-equation will be dominated by the numerator. The explicit dependence on $q_r^{(0)}$ will induce a Burgers-type advective nonlinearity, whereas the appearance of $\partial_z q_r^{(0)}$ induces a Hamilton–Jacobi-type term. In fact, with obvious abbreviations we have

$$w^{(0)} = a q_r^{(0)} - b \partial_z q_r^{(0)} \tag{119}$$

and, neglecting horizontal derivatives for simplicity, the equation for q_r reads

$$\partial_t q_r^{(0)} + \left(a q_r^{(0)} - b\frac{\mathrm{d}q_{\mathrm{vs}}^{(0)}}{\mathrm{d}z} - V_r\right)\partial_z q_r^{(0)} - b(\partial_z q_r^{(0)})^2 = -\left(a\frac{\mathrm{d}q_{\mathrm{vs}}^{(0)}}{\mathrm{d}z} + V_r\right) q_r^{(0)}. \tag{120}$$

5.3.3 Undersaturated air

In undersaturated regions within a narrow tower, all cloud water will rapidly evaporate, so that $q_c^{(0)} \equiv 0$. Precipitation that descends into an undersaturated region will evaporate at a rate of order unity on the time scale considered here, so that the remaining moisture variables q_v, q_r to leading order satisfy the transport equations

$$D_t^{(0)} q_v^{(0)} = S_{\mathrm{ev}}^{(0)}, \tag{121}$$

$$D_t^{(0)} q_r^{(0)} - \frac{1}{\rho_0}\partial_z\left(\rho_0 q_r^{(0)} V_r\right) = -S_{\mathrm{ev}}^{(0)}, \tag{122}$$

where

$$S_{\mathrm{ev}}^{(0)} = L C_{\mathrm{ev}}\left(q_{\mathrm{vs}}^{(0)} - q_v^{(0)}\right) q_r^{(0)}. \tag{123}$$

In the undersaturated regions, the rather strong stability associated with the moist adiabatic potential temperature distribution is not overcome by matching latent heat release from condensation as it is in the saturated

region. As a consequence, the vertical velocity is determined, as in the "weak temperature gradient approximation" [1,16,17], by the quasi-steady form of the potential temperature transport equation,

$$w^{(0)}\frac{\mathrm{d}\theta^{(1)}}{\mathrm{d}z} = -LS_{\mathrm{ev}}^{(0)} = -LC_{\mathrm{ev}}\left(q_{\mathrm{vs}}^{(0)} - q_v^{(0)}\right)q_r^{(0)}. \tag{124}$$

5.4 Differences between the moist thermodynamics scaling regimes

Although the asymptotic approximations to the moist adiabatic distribution were comparably accurate for the two distinguished limit regimes from Table 2 (see Fig. 1), there are subtle differences for the approximate dynamics of a narrow tower. Taking into account the different scaling regimes labeled $\alpha = 0$ and $\alpha = 1$ in Table 2, we obtain for the expansion of the density potential temperature,

$$\begin{aligned}\theta_\rho = 1 + \varepsilon\Big(\theta^{(1)} + \frac{1-\alpha}{E}q_v^{(0)}\Big) \\ + \varepsilon^2\left(\theta^{(2)} + \frac{1-\alpha}{E}q_v^{(1)} + \left(\frac{\alpha}{E} - 1\right)q_v^{(0)} - q_c^{(0)} - q_r^{(0)}\right)\Big) + O(\varepsilon^3)\end{aligned} \tag{125}$$

For $\alpha = 0$ we obtain therefore from the vertical momentum balance to $O(\varepsilon^{-2})$ the additional condition

$$0 = -\frac{\widetilde{\rho}^{(1)}}{p^{(0)}} = \widetilde{\theta}_\rho^{(1)} = \frac{1-\alpha}{E}\widetilde{q}_v^{(0)} \tag{126}$$

implying $q_v^{(0)} \equiv \bar{q}_v^{(0)}$. Since we want to allow for saturation at least within the core of a narrow cloud tower, this results in the condition

$$q_v^{(0)} \equiv q_{\mathrm{vs}}^{(0)}. \tag{127}$$

This amounts to the air being close to saturation in the environment of a tower, i.e., on a scale of $\sim 10\,\mathrm{km}$. This is not uncommon in the tropics but restricts the applicability of the $\alpha = 0$-regime. A distinction between saturated and undersaturated air is then made based upon the first-order components,

$$\begin{array}{lll}\text{saturated} & : & q_v^{(1)} \equiv q_{\mathrm{vs}}^{(1)} \\ \text{undersaturated} & : & q_v^{(1)} < q_{\mathrm{vs}}^{(1)} \text{ with } q_{\mathrm{vs}}^{(1)} - q_v^{(1)} = O(1)\end{array}$$

Since in the present hot tower setting the regime $\alpha = 0$ requires this restriction of almost saturation everywhere, we discuss here the differences between both scaling regimes in this particular setting and assume (127) to hold throughout this subsection. The difference in the regimes then enters via the diagnostic relation from the buoyancy to second order

$$0 = \widetilde{\theta}_\rho^{(2)} = \widetilde{\theta}^{(2)} + \frac{1-\alpha}{E}\widetilde{q}_v^{(1)} - q_c^{(0)} - q_r^{(0)}. \tag{128}$$

The fact that the $\alpha = 0$ scaling regime would restrict applicability of the entire theory to near-saturated local environments while for $\alpha = 1$ the theory would be applicable under more general conditions points toward the latter as the more attractive scaling regime.

5.4.1 Saturated air

In saturated air, as mentioned above, we have $q_v^{(1)} \equiv q_{vs,1}$. For the cloud water mixing ratio we obtain, in analogy with the earlier calculations

$$q_c^{(0)} = 0\,, \qquad C_{\mathrm{cr}}q_c^{(1)}q_r^{(0)} = -w^{(0)}\frac{\mathrm{d}q_{\mathrm{vs}}^{(0)}}{\mathrm{d}z}. \tag{129}$$

The leading order rain dynamics is the same for both scaling regimes as well,

$$D_t^{(0)}q_r^{(0)} - \frac{1}{\rho_0}\partial_z\left(\rho^{(0)}q_r^{(0)}V_r\right) = -w^{(0)}\frac{\mathrm{d}q_{\mathrm{vs}}^{(0)}}{\mathrm{d}z}. \tag{130}$$

Also the equation for the potential temperature fluctuation is again as before

$$D_t^{(0)}\widetilde{\theta}^{(2)} = w^{(0)}\frac{\mathrm{d}\Delta\Theta^{(2)}}{\mathrm{d}z} + k_l q_r^{(0)}\left(V_r - w^{(0)}\right)\frac{\mathrm{d}T^{(1)}}{\mathrm{d}z}. \tag{131}$$

Inserting now the balance equation from the buoyancy to second order (128), we obtain different relations for the vertical velocity

$$\begin{aligned} &w^{(0)}\left(k_l q_r^{(0)}\frac{\mathrm{d}T^{(1)}}{\mathrm{d}z} - \frac{\mathrm{d}\Delta\Theta^{(2)}}{\mathrm{d}z} - \frac{1-\alpha}{E}\frac{\mathrm{d}\Delta Q_v^{(1)}}{\mathrm{d}z} - \frac{\mathrm{d}q_{\mathrm{vs}}^{(0)}}{\mathrm{d}z}\right) \\ &\quad = k_l q_r^{(0)} V_r \frac{\mathrm{d}T^{(1)}}{\mathrm{d}z} - \frac{V_r}{\rho_0}\partial_z\left(\rho^{(0)} q_r^{(0)}\right), \end{aligned} \tag{132}$$

where $\Delta Q_v^{(1)} = q_{\mathrm{vs}}^{(1)} - \overline{q}_v^{(1)}$.

5.4.2 Undersaturated air

In undersaturated air we have $q_c \equiv 0$ and $q_v^{(1)} < q_{\mathrm{vs}}^{(1)}$. Moreover, we note that due to the condition of everywhere almost saturation in (127), the evaporation vanishes to leading order and we have

$$S_{\mathrm{ev}}^{(0)} = 0 \qquad \text{and} \qquad S_{\mathrm{ev}}^{(1)} = C_{\mathrm{ev}}\left(q_{\mathrm{vs}}^{(1)} - q_v^{(1)}\right)^+ q_r^{(0)}. \tag{133}$$

The strategy of obtaining the different solution components differs here from the previous setting for scaling regime 1. In particular, we obtain the vanishing of the vertical velocity to leading order from the equation for water vapor using (127) and (133)

$$w^{(0)}\frac{\mathrm{d}q_{\mathrm{vs}}^{(0)}}{\mathrm{d}z} = 0 \qquad \text{implying} \qquad w^{(0)} = 0. \tag{134}$$

To next order we obtain

$$D_t^{(0)} q_v^{(1)} + w^{(1)}\frac{\mathrm{d}q_{\mathrm{vs}}^{(0)}}{\mathrm{d}z} = S_{\mathrm{ev}}^{(1)}. \tag{135}$$

Due to the weak evaporation the rain water is also merely transported to leading order

$$D_t^{(0)} q_r^{(0)} - \frac{1}{\rho_0}\partial_z\left(\rho_0 q_r^{(0)} V_r\right) = 0. \tag{136}$$

To close the dynamics we still need to determine $w^{(1)}$, which we obtain again from the potential temperature equation. In the undersaturated region the latter reduces for $w^{(0)} = 0$ to

$$D_t^{(0)}\widetilde{\theta}^{(2)} + w^{(1)}\frac{\mathrm{d}\theta^{(1)}}{\mathrm{d}z} = k_l q_r^{(0)} V_r \frac{\mathrm{d}T^{(1)}}{\mathrm{d}z} - L S_{\mathrm{ev}}^{(1)}. \tag{137}$$

Note that averaging this equation in particular implies $\overline{w}^{(1)} = 0$ and thus also $\partial_t \overline{q_v}^{(1)} = 0$. Therefore, using (128) and (90) we can solve this equation for $w^{(1)}$ as follows

$$\left(\frac{1-\alpha}{E} - L\right)\frac{\mathrm{d}q_{\mathrm{vs}}^{(0)}}{\mathrm{d}z} w^{(1)} = \left(\frac{1-\alpha}{E} - L\right) S_{\mathrm{ev}}^{(1)} + V_r\left(k_l \frac{\mathrm{d}T^{(1)}}{\mathrm{d}z} q_r^{(0)} - \frac{1}{\rho_0}\partial_z(\rho^{(0)} q_r^{(0)})\right). \tag{138}$$

6 Up- and downdrafts on the convection time scale

Here we present sample numerical solutions for the up- and downdraft models derived in Sects. 6.1 and 6.2, respectively. We restrict to the simplest settings, neglecting horizontal advection within the towers as well as (turbulent) transport, to reveal the essential behavior of the convective scale dynamics equations. The construction and investigation of a self-consistent tower model in which both regimes will be coupled by turbulent transport, and a thorough comparison with existing turbulent plume and buoyant bubble models for individual deep convection events is left for future work.

6.1 Updrafts

Here we solve the Hamilton–Jacobi-type equation (120) for updrafts in saturated parts of a tower and for the asymptotic scaling regime $\alpha = 1$ from Table 2,

$$\partial_t q_r^{(0)} + \left(a q_r^{(0)} - b \frac{dq_{\rm vs}^{(0)}}{\mathrm{d}z} - V_r \right) \partial_z q_r^{(0)} - b (\partial_z q_r^{(0)})^2 = - \left(a \frac{\mathrm{d}q_{\rm vs}^{(0)}}{\mathrm{d}z} + V_r \right) q_r^{(0)} , \tag{139}$$

where the coefficients a, b are given by

$$a = \frac{V_r}{D} \left[k_l \frac{\mathrm{d}T^{(1)}}{\mathrm{d}z} + 1 \right] , \qquad b = \frac{V_r}{D} \tag{140}$$

with

$$D = k_l \frac{\mathrm{d}T^{(1)}}{\mathrm{d}z} q_r^{(0)} - \frac{\mathrm{d}\Delta\Theta^{(2)}}{\mathrm{d}z} - \frac{1}{E} \frac{\mathrm{d}q_{\rm vs}^{(0)}}{\mathrm{d}z} + \left(\frac{1}{E} - 1 \right) \frac{\mathrm{d}\overline{q}_v^{(0)}}{\mathrm{d}z} . \tag{141}$$

The equation is solved using Strang splitting between the Hamilton–Jacobi terms involving the vertical derivative $\partial_z q_r^{(0)}$ on the left, and the source term proportional to $q_r^{(0)}$ on the right. For the first split step we have adapted the first-order finite difference scheme for Hamilton–Jacobi equations by Crandall–Lions, [27]. The second split step has an obvious analytical solution, namely

$$q_{r\,i}^{\,n+1} = q_{r\,i}^{\,n} \exp \left(- \left[a \frac{\mathrm{d}q_{\rm vs}}{\mathrm{d}z} + V_r \right] \Delta t \right) , \tag{142}$$

where we have dropped the $^{(0)}$ superscript for convenience of notation, and where $q_{r\,i}^{\,n}$ denotes the approximate numerical value for $q_r^{(0)}$ at time level $t^n = n\Delta t$ and grid location $z_i = i\,\Delta z$.

Figure 4 gives an impression of the implications of the saturated tower dynamical equations by comparing the rain water dynamics with and without the self-induced vertical velocity from (118). Both simulations start from initial data

$$q_r(0, z) = \begin{cases} 0.125\, q_{vs}^{(0)}(z)\, (1 + \cos(\pi z)) & (0 \le z \le 1) \\ 0 & \text{otherwise} \end{cases} \tag{143}$$

The left triple of graphs shows snapshots of vertical profiles of $q_r^{(0)}$, $q_r^{(0)}/q_{vs}^{(0)}$, and $w^{(0)}$ as they evolve under Eq. (139) for times $0 \le t \le 4.2$. The right triple of graphs shows similar snapshots when the self-induced

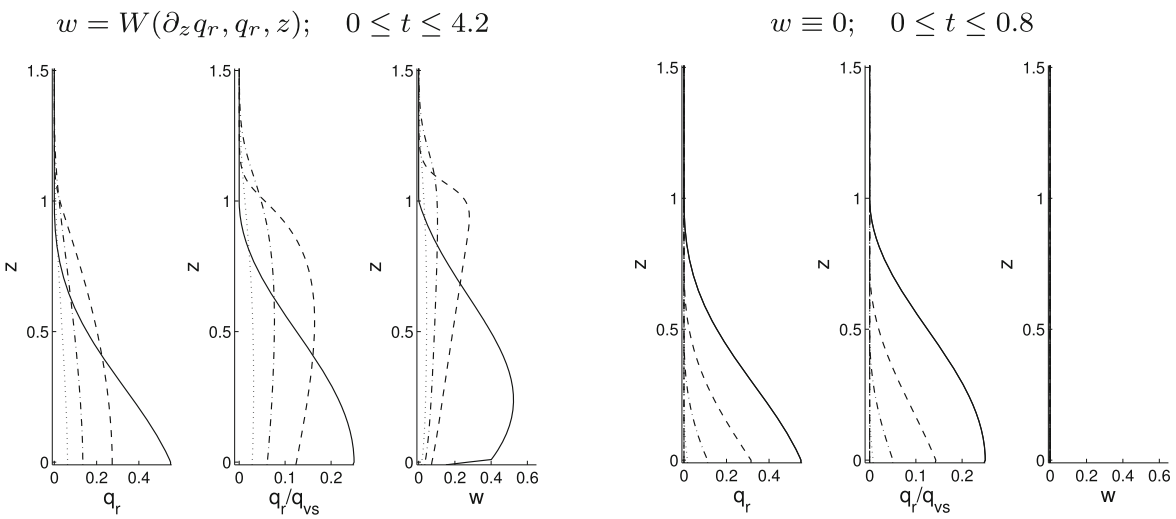

Fig. 4 Evolution of rain water mixing ratio and vertical velocity with (*left column*) and without (*right column*) the self-induced vertical velocity from (118). Output times in the left set of *graphs*: *solid* $t = 0$, *dashed* $t = 1.378$, *dash-dotted* $t = 2.75$, *dotted* $t = 4.13$. Output times on the right: *solid* $t = 0$, *dashed* $t = 0.26$, *dash-dotted* $t = 0.51$, *dotted* $t = 0.77$

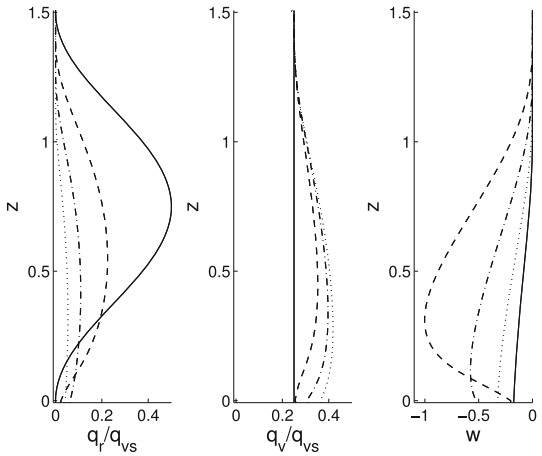

Fig. 5 Evolution of rain water mixing ratio and vertical velocity in undersaturated air. Output times: *solid* $t = 0$, *dashed* $t = 0.13$, *dash-dotted* $t = 0.25$, *dotted* $t = 0.38$

vertical velocity is set to zero, so that the rain water simply precipitates with the terminal sedimentation velocity $-V_r$. The rain falls down rather rapidly in this case, so that we show snapshots within the interval $0 \le t \le 0.8$ in these graphs. Comparing the left and right sets of graphs we observe that the self-induced updraft tends to substantially prolong the life time of a convective tower, and this also implies much higher precipitation yield.

6.2 Downdrafts

Here we provide an example of the evolution of the water constituents and the vertical velocity in undersaturated regions of a cloud tower following Eqs. (121)–(124). The calculations start from initial data

$$\left.\begin{aligned} q_r(0,z) &= 0.25\, q_{vs}^{(0)}(z)(1-\cos(4\pi z/3)) \\ q_v(0,z) &= 0.25\, q_{vs}^{(0)}(z) \end{aligned}\right\} \qquad (0 \le z \le 3/2) \tag{144}$$

and cover a rather short time interval of $0 \le t \le 0.4$. As expected, we see the precipitation descend and evaporate in the leftmost graph. It therefore moistens the atmosphere as seen in the middle graph where the relative humidity q_v/q_{vs} increases by a factor of roughly two in the lower parts of the domain in the course of time. The descent of the rain water is pronounced here further in comparison with the saturated, updraft-free case discussed in the context of Fig. 4, right triple of graphs, by the downdraft velocity induced by evaporative cooling (rightmost graph in Fig. 5). This is why the present process is already completed essentially after dimensionless times of order $t \sim 0.5$.

7 Conclusions

In this paper we have presented two alternative scaling regimes that allow us to incorporate a familiar class of bulk moist microphysics closures in the general multiscale asymptotic modeling framework for atmospheric flows summarized in [8]. A first application of these, quite similar, scaling regimes to the dynamics of convective hot towers revealed a mechanism of self-sustained precipitating updrafts in saturated air, and it provided an asymptotic description of strong downdrafts due to evaporative cooling in undersaturated air.

This first application is as yet rudimentary, however, since we have set aside the issue of stability of the quasi-steady balances that characterize the considered flow regimes, three-dimensional advection within the cloud towers, turbulent transport, lateral entrainment, the interaction of adjacent cloud towers, the influence of bottom boundary layers, and the large-scale organization of ensembles of hot towers. All these aspects shall be addressed in forthcoming publications.

Acknowledgements The authors thank Olivier Pauluis (Courant Institute) for helpful discussions on the thermodynamics of moist air, and the Institute for Pure and Applied Mathematics (IPAM) at UCLA for hosting the Long Term Program *Model and*

Data Hierarchies for Simulating and Understanding Climate in 2010. In the course of this program the authors were able to lay the foundations for the present collaboration. S.H. thanks the Austrian Science Fund for their support via the Hertha-Firnberg project T-764. R.K. acknowledges support by the Deutsche Forschungsgemeinschaft through the Collaborative Research Center CRC 1114 "Scaling Cascades in Complex Systems," Project C06. The authors gratefully acknowledge the fabulous work of developers and maintainers of the free LaTeX word processing system and of the TeXShop TeX-writing environment.

A Derivation of the scaled moist adiabatic equation (75)

A.1 Effective equation for the moist adiabat

Inserting the hydrostatic equation (71) into (70), the equations for the moist adiabat become

$$\frac{\mathrm{d}\ln\theta}{\mathrm{d}z} = -\varepsilon^{e-a}\frac{L\phi_\varepsilon(T)}{C_\varepsilon\pi\theta}\frac{\mathrm{d}}{\mathrm{d}z}q_{\mathrm{vs}}(\theta,\pi;\varepsilon) + \varepsilon^{e}\frac{\Sigma_\varepsilon\Psi_\varepsilon(q_{\mathrm{vs}})}{C_\varepsilon}\frac{1}{\pi\theta} \tag{145}$$

$$\frac{\mathrm{d}\ln\pi}{\mathrm{d}z} = -\varepsilon^{b}\frac{\Gamma}{\pi\theta}\Psi_\varepsilon(q_{\mathrm{vs}}) \tag{146}$$

where

$$\Psi_\varepsilon(q_{\mathrm{vs}}) = \frac{1+\varepsilon^e q_{\mathrm{vs}}}{1+\varepsilon^{e-c}q_{\mathrm{vs}}/E} \tag{147}$$

$$C_\varepsilon = 1+\varepsilon^{e+b-b_v-c}\frac{\Gamma}{E\Gamma_v}q_{\mathrm{vs}} \tag{148}$$

$$\Sigma_\varepsilon = \varepsilon^{b-c}\frac{\Gamma}{E}\Big(\varepsilon^{b-b_v}\frac{\Gamma}{\Gamma_v}-1\Big)q_{\mathrm{vs}} \tag{149}$$

In the sequel we are interested in the dominant contributions in these equations, so we keep only the leading order terms. That is, we drop the second term on the right in (145), and set $C_\varepsilon = \Psi_\varepsilon \equiv 1$ in the first terms of (145) and (146) and obtain

$$\frac{\mathrm{d}\ln\theta}{\mathrm{d}z} = -\varepsilon^{e-a}\frac{L\phi_\varepsilon(T)}{\pi\theta}\frac{\mathrm{d}}{\mathrm{d}z}\widehat{q}_{\mathrm{vs}}(\theta,\pi;\varepsilon) \tag{150}$$

$$\frac{\mathrm{d}\ln\pi}{\mathrm{d}z} = -\varepsilon^{b}\frac{\Gamma}{\pi\theta} \tag{151}$$

This is the starting point for the subsequent scale analysis.
For the saturation water vapor mixing ratio, q_{vs}, the dependence on the unknowns θ, π follows from the definition of e_s in (69) which depends on temperature only, so that – with $T = \pi\theta$ –

$$\widehat{q}_{\mathrm{vs}}(\theta,\pi;\varepsilon) = \frac{E\widehat{e}_s(T;\varepsilon)}{p-\varepsilon^{e-c}\widehat{e}_s(T;\varepsilon)} \equiv \frac{E\widehat{e}_s(\theta\pi;\varepsilon)}{\pi^{1/\varepsilon^b\Gamma}-\varepsilon^{e-c}\widehat{e}_s(\theta\pi;\varepsilon)} \tag{152}$$

where the Clausius–Clapeyron relation for $\widehat{e}_s$ reads as

$$\frac{1}{\widehat{e}_s}\frac{\mathrm{d}\widehat{e}_s}{\mathrm{d}T} = \frac{1}{\varepsilon^d}\frac{AL}{T^2}\phi_\varepsilon(T) \tag{153}$$

with $\phi_\varepsilon(T)$ from (59). Evaluation of $\mathrm{d}\widehat{q}_{\mathrm{vs}}/\mathrm{d}z$ on the r.h.s. of (145) yields

$$\frac{\mathrm{d}\widehat{q}_{\mathrm{vs}}}{\mathrm{d}z} = \left[\frac{\partial\widehat{q}_{\mathrm{vs}}}{\partial\pi}\frac{\mathrm{d}\pi}{\mathrm{d}z}+\frac{\partial\widehat{q}_{\mathrm{vs}}}{\partial\theta}\frac{\mathrm{d}\theta}{\mathrm{d}z}\right]. \tag{154}$$

Re-inserted into (145) and using (146) we find

$$\left[1+\varepsilon^{e-a}\frac{L\phi_\varepsilon}{\pi}\frac{\partial\widehat{q}_{\mathrm{vs}}}{\partial\theta}\right]\frac{\mathrm{d}\theta}{\mathrm{d}z} = \varepsilon^{e-a}\frac{L\phi_\varepsilon}{\pi}\frac{\partial\widehat{q}_{\mathrm{vs}}}{\partial\pi}\frac{\varepsilon^b\Gamma}{\theta}. \tag{155}$$

Using (73), the two partial derivatives of q_{vs} become

$$\begin{aligned}
\frac{\partial \widehat{q}_{\text{vs}}}{\partial \theta} &= \left[\frac{\widehat{q}_{\text{vs}}}{\widehat{e}_s} + \frac{\varepsilon^{e-c}\widehat{q}_{\text{vs}}}{p-\varepsilon^{e-c}\widehat{e}_s}\right]\frac{\partial \widehat{e}_s}{\partial \theta} = \left[\frac{\widehat{q}_{\text{vs}}}{\widehat{e}_s} + \frac{\varepsilon^{e-c}\widehat{q}_{\text{vs}}}{p-\varepsilon^{e-c}\widehat{e}_s}\right]\pi\frac{\mathrm{d}\widehat{e}_s}{dT} \\
&= \left[\frac{\widehat{q}_{\text{vs}}}{\widehat{e}_s} + \frac{\varepsilon^{e-c}\widehat{q}_{\text{vs}}}{p-\varepsilon^{e-c}\widehat{e}_s}\right]\frac{\pi\widehat{e}_s}{\varepsilon^d}\frac{AL\phi_\varepsilon}{T^2} = \left[\frac{p}{p-\varepsilon^{e-c}\widehat{e}_s}\right]\frac{\pi}{\varepsilon^d}\frac{AL\phi_\varepsilon}{T^2}\widehat{q}_{\text{vs}} \\
&= \mathcal{O}\left(\varepsilon^{-d}\right) \qquad (\varepsilon\to 0)
\end{aligned} \tag{156}$$

$$\begin{aligned}
\frac{\partial \widehat{q}_{\text{vs}}}{\partial \pi} &= \left[-\frac{\widehat{q}_{\text{vs}}}{p-\varepsilon^{e-c}\widehat{e}_s}\right]\frac{\mathrm{d}p}{d\pi} + \left[\frac{\widehat{q}_{\text{vs}}}{\widehat{e}_s} + \frac{\varepsilon^{e-c}\widehat{q}_{\text{vs}}}{p-\varepsilon^{e-c}\widehat{e}_s}\right]\frac{\partial \widehat{e}_s}{\partial \pi} \\
&= \left[-\frac{\widehat{q}_{\text{vs}}}{p-\varepsilon^{e-c}\widehat{e}_s}\right]\frac{\mathrm{d}\pi^{1/\varepsilon^b\Gamma}}{d\pi} + \left[\frac{\widehat{q}_{\text{vs}}}{\widehat{e}_s} + \frac{\varepsilon^{e-c}\widehat{q}_{\text{vs}}}{p-\varepsilon^{e-c}\widehat{e}_s}\right]\theta\frac{\mathrm{d}\widehat{e}_s}{\mathrm{d}T} \\
&= \left[\frac{p}{p-\varepsilon^{e-c}\widehat{e}_s}\right]\left(\frac{\theta}{\varepsilon^d}\frac{AL\phi_\varepsilon}{T^2} - \frac{1}{\varepsilon^b\Gamma\pi}\right)\widehat{q}_{\text{vs}} \\
&= \mathcal{O}\left(\varepsilon^{-b},\varepsilon^{-d}\right) \qquad (\varepsilon\to 0)
\end{aligned} \tag{157}$$

Collecting the results from (155), (156), and (157) we have

$$\begin{aligned}
\frac{\mathrm{d}\theta}{\mathrm{d}z} &= \varepsilon^b\frac{\Gamma}{\theta}\frac{\left[\frac{p}{p-\varepsilon^{e-c}\widehat{e}_s}\right]\left(\frac{\theta}{\varepsilon^{d-e}}\frac{AL\phi_\varepsilon}{T^2} - \frac{1}{\varepsilon^{b-e}}\frac{1}{\Gamma\pi}\right)\widehat{q}_{\text{vs}}}{\left[\frac{p}{p-\varepsilon^{e-c}\widehat{e}_s}\right]\frac{\pi}{\varepsilon^{d-e}}\frac{AL\phi_\varepsilon}{T^2}\widehat{q}_{\text{vs}} + \frac{\varepsilon^a\pi}{L\phi_\varepsilon}} \\
&= \varepsilon^b\frac{\Gamma}{\pi}\frac{\left(\frac{AL\phi_\varepsilon}{T^2} - \frac{\varepsilon^{d-b}}{\Gamma\theta\pi}\right)\widehat{q}_{\text{vs}}}{\frac{AL\phi_\varepsilon}{T^2}\widehat{q}_{\text{vs}} + \frac{\varepsilon^{a+d-e}I_\varepsilon}{L\phi_\varepsilon}} \qquad \left(I_\varepsilon \equiv 1 - \frac{\varepsilon^{e-c}\widehat{e}_s}{p}\right) \\
&= \varepsilon^b\frac{\Gamma}{\pi}\left(1-\varepsilon^{a+d-e}\frac{I_\varepsilon + \varepsilon^{e-a-b}\frac{L\phi_\varepsilon}{\Gamma T}\widehat{q}_{\text{vs}}}{\frac{AL^2\phi_\varepsilon^2}{T^2}\widehat{q}_{\text{vs}} + \varepsilon^{a+d-e}I_\varepsilon}\right)
\end{aligned} \tag{158}$$

The hindsight check of validity of the truncations we introduced in going from (145), (146) to the simpler system (150), (151), given the final results for the various exponents in (66) of the scale analysis in Sect. 4.1, *i.e.*,

$$a = b = b_v = c = 1\,, \qquad \text{and} \qquad e = 2 \tag{159}$$

shows that $\varepsilon^e \ll \varepsilon^{e-a}$, $\varepsilon^{e+b-b_v-c} = \varepsilon^{e-c} = \varepsilon \ll 1$, and that justifies the approximations introduced.

B Asymptotics of the moist adiabat

B.1 Expansion of the balance equations for the moist adiabat

We recall that scaling regime 1 amounts to $\alpha = 1$ and scaling regime 2 to $\alpha = 0$. The following derivations are valid for both regimes, where in the expansions we account for the different regimes by making use of the switching function $(1-\alpha)$ as a prefactor for terms, which vanish in regime 1, but are present in regime 2. For the moist adiabat (i.e., at saturation without liquid water) we have the balance equations

$$\frac{\mathrm{d}\theta}{\mathrm{d}z} = -\varepsilon\frac{L\phi_\varepsilon(T)}{C_\varepsilon\pi}\frac{\mathrm{d}}{\mathrm{d}z}q_{\text{vs}}(\theta,\pi;\varepsilon) + \varepsilon^2\frac{\Sigma_\varepsilon\Psi_\varepsilon(q_{\text{vs}})}{C_\varepsilon\pi} \tag{160}$$

$$\frac{\mathrm{d}\pi}{\mathrm{d}z} = -\varepsilon\frac{\Gamma}{\theta}\Psi_\varepsilon(q_{\text{vs}}) \tag{161}$$

where

$$\Psi_\varepsilon(q_{\text{vs}}) = \frac{1+\varepsilon^2 q_{\text{vs}}}{1+\varepsilon^{1+\alpha}\,q_{\text{vs}}/E} \tag{162}$$

$$C_\varepsilon = 1+\varepsilon^{1+\alpha}\,k_v q_{\text{vs}} \tag{163}$$

$$\Sigma_\varepsilon = \varepsilon^\alpha\kappa_v q_{\text{vs}} \tag{164}$$

We insert the expansions

$$\theta = 1+\varepsilon\theta^{(1)}+\varepsilon^2\theta^{(2)}+o\left(\varepsilon^2\right) \tag{165}$$

$$\pi = 1+\varepsilon\pi^{(1)}+\varepsilon^2\pi^{(2)}+o\left(\varepsilon^2\right) \tag{166}$$

$$q_{\text{vs}} = q_{\text{vs}}^{(0)}+\varepsilon q_{\text{vs}}^{(1)}+o\left(\varepsilon\right)\,, \tag{167}$$

of the unknowns into (160), (161) to obtain

$$\frac{\mathrm{d}\theta^{(1)}}{\mathrm{d}z} = -L\frac{\mathrm{d}q_{\mathrm{vs}}^{(0)}}{\mathrm{d}z} \tag{168}$$

$$\frac{\mathrm{d}\pi^{(1)}}{\mathrm{d}z} = -\Gamma \tag{169}$$

$$\frac{\mathrm{d}\theta^{(2)}}{\mathrm{d}z} = -L\frac{\mathrm{d}q_{\mathrm{vs}}^{(1)}}{\mathrm{d}z} + L\frac{\mathrm{d}q_{\mathrm{vs}}^{(0)}}{\mathrm{d}z}\left(\chi T^{(1)} + \pi^{(1)} + (1-\alpha)k_v q_{\mathrm{vs}}^{(0)}\right) + (1-\alpha)\kappa_v q_{\mathrm{vs}}^{(0)}. \tag{170}$$

$$\frac{\mathrm{d}\pi^{(2)}}{\mathrm{d}z} = \Gamma\left(\theta^{(1)} + (1-\alpha)q_{\mathrm{vs}}^{(0)}/E\right) \tag{171}$$

To close (168) we recall the constitutive equation for q_{vs}, *i.e.*,

$$q_{\mathrm{vs}} = \frac{E e_s(T)}{p - \varepsilon^{1+\alpha} e_s(T)} \qquad \text{where } e_s(T) \text{ satisfies} \qquad \frac{\mathrm{d}\ln e_s}{\mathrm{d}T} = \frac{AL}{\varepsilon}\frac{\phi_\varepsilon(T)}{T^2}. \tag{172}$$

This leads to

$$\begin{aligned}
\frac{\mathrm{d}q_{\mathrm{vs}}}{\mathrm{d}z} &= \left[\frac{q_{\mathrm{vs}}}{e_s} + \frac{\varepsilon^{1+\alpha} q_{\mathrm{vs}}}{p - \varepsilon^{1+\alpha} e_s}\right]\frac{\mathrm{d}e_s}{\mathrm{d}T}\frac{\mathrm{d}T}{\mathrm{d}z} - \left[\frac{q_{\mathrm{vs}}}{p - \varepsilon^{1+\alpha} e_s}\right]\frac{\mathrm{d}p}{\mathrm{d}z} \\
&= q_{\mathrm{vs}}\left[1 + \frac{\varepsilon^{1+\alpha} e_s}{p - \varepsilon^{1+\alpha} e_s}\right]\frac{\mathrm{d}\ln e_s}{\mathrm{d}T}\frac{\mathrm{d}T}{\mathrm{d}z} - q_{\mathrm{vs}}\left[\frac{p}{p - \varepsilon^{1+\alpha} e_s}\right]\frac{\mathrm{d}\ln p}{\mathrm{d}z} \\
&= q_{\mathrm{vs}}\left[\frac{1}{1 - \varepsilon^{1+\alpha} e_s/p}\right]\left(\frac{AL}{\varepsilon}\frac{\phi_\varepsilon(T)}{T}\frac{\mathrm{d}\ln T}{\mathrm{d}z} - \frac{1}{\varepsilon\Gamma}\frac{\mathrm{d}\ln \pi}{\mathrm{d}z}\right) \\
&= q_{\mathrm{vs}}\left[\frac{1}{1 - \varepsilon^{1+\alpha} e_s/p}\right]\left(\frac{AL\phi_\varepsilon(T)}{T}\left(\frac{1}{\theta}\frac{\mathrm{d}\widetilde{\theta}}{\mathrm{d}z} + \frac{1}{\pi}\frac{\mathrm{d}\widetilde{\pi}}{\mathrm{d}z}\right) - \frac{1}{\Gamma\pi}\frac{\mathrm{d}\widetilde{\pi}}{\mathrm{d}z}\right)
\end{aligned} \tag{173}$$

where we have used that $T = \pi\theta$ and introduced the abbreviations $\theta = 1 + \varepsilon\widetilde{\theta}$ and $\pi = 1 + \varepsilon\widetilde{\pi}$. Expanding this result to leading and first order we find

$$\frac{\mathrm{d}q_{\mathrm{vs}}^{(0)}}{\mathrm{d}z} = q_{\mathrm{vs}}^{(0)}\left(AL\frac{\mathrm{d}\theta^{(1)}}{\mathrm{d}z} + \frac{AL\Gamma - 1}{\Gamma}\frac{\mathrm{d}\pi^{(1)}}{\mathrm{d}z}\right) \tag{174}$$

$$\begin{aligned}
\frac{\mathrm{d}q_{\mathrm{vs}}^{(1)}}{\mathrm{d}z} &= \left(q_{\mathrm{vs}}^{(1)} + (1-\alpha)q_{\mathrm{vs}}^{(0)}\left(\frac{e_s}{p}\right)^{(0)}\right)\left(AL\frac{\mathrm{d}\theta^{(1)}}{\mathrm{d}z} + \frac{AL\Gamma - 1}{\Gamma}\frac{\mathrm{d}\pi^{(1)}}{\mathrm{d}z}\right) \\
&\quad + q_{\mathrm{vs}}^{(0)}\left(AL\frac{\mathrm{d}\theta^{(2)}}{\mathrm{d}z} + \frac{AL\Gamma - 1}{\Gamma}\frac{\mathrm{d}\pi^{(2)}}{\mathrm{d}z}\right) \\
&\quad - q_{\mathrm{vs}}^{(0)} AL\,(\chi + 1)\,T^{(1)}\left(\frac{\mathrm{d}\theta^{(1)}}{\mathrm{d}z} + \frac{\mathrm{d}\pi^{(1)}}{\mathrm{d}z}\right) \\
&\quad + q_{\mathrm{vs}}^{(0)}\left(-AL\left[\theta^{(1)}\frac{\mathrm{d}\theta^{(1)}}{\mathrm{d}z} + \pi^{(1)}\frac{\mathrm{d}\pi^{(1)}}{\mathrm{d}z}\right] + \frac{\pi^{(1)}}{\Gamma}\frac{\mathrm{d}\pi^{(1)}}{\mathrm{d}z}\right)
\end{aligned} \tag{175}$$

B.2 Leading order moist adiabatic solution

Equation (169) is readily solved by

$$\pi^{(1)} = -\Gamma z. \tag{176}$$

Re-inserting (168) into the (174) we find a closed equation for $q_{\mathrm{vs}}^{(0)}$,

$$\frac{\mathrm{d}q_{\mathrm{vs}}^{(0)}}{\mathrm{d}z} = -\frac{(AL\Gamma - 1)q_{\mathrm{vs}}^{(0)}}{AL^2 q_{\mathrm{vs}}^{(0)} + 1} \tag{177}$$

which is readily solved by (89), *i.e.*,

$$\ln\left(\frac{q_{\mathrm{vs}}^{(0)}}{q_{\mathrm{vs}\,0}^{(0)}}\right) + AL^2\left(q_{\mathrm{vs}}^{(0)} - q_{\mathrm{vs}\,0}^{(0)}\right) = -(AL\Gamma - 1)z, \tag{178}$$

With these results we also have

$$\theta^{(1)} = -L\left(q_{\mathrm{vs}}^{(0)}(z) - q_{\mathrm{vs}}^{(0)}(0)\right) \tag{179}$$

$$T^{(1)} = \theta^{(1)} + \pi^{(1)} = \theta^{(1)} - \Gamma z. \tag{180}$$

B.3 First-order moist adiabatic solution

Next we reconsider (175) using (174) and (177) to obtain

$$\begin{aligned}\frac{\mathrm{d}q_{\mathrm{vs}}^{(1)}}{\mathrm{d}z} &= \left(\frac{q_{\mathrm{vs}}^{(1)}}{q_{\mathrm{vs}}^{(0)}} + (1-\alpha)\left(\frac{e_s}{p}\right)^{(0)}\right)\frac{\mathrm{d}q_{\mathrm{vs}}^{(0)}}{\mathrm{d}z} \\ &\quad + q_{\mathrm{vs}}^{(0)}\left(AL\frac{\mathrm{d}\theta^{(2)}}{\mathrm{d}z} + \frac{AL\Gamma - 1}{\Gamma}\frac{\mathrm{d}\pi^{(2)}}{\mathrm{d}z}\right) \\ &\quad - q_{\mathrm{vs}}^{(0)}\left(\frac{AL}{2}\left[(\chi+1)\frac{\mathrm{d}T^{(1)^2}}{\mathrm{d}z} + \frac{\mathrm{d}\theta^{(1)^2}}{\mathrm{d}z}\right] + \frac{AL\Gamma - 1}{2\Gamma}\frac{\mathrm{d}\pi^{(1)^2}}{\mathrm{d}z}\right)\end{aligned} \tag{181}$$

This is recast collecting the terms involving $q_{\mathrm{vs}}^{(1)}$, $\theta^{(2)}$, and $\pi^{(2)}$ on the left and using that (172) can be solved for e_s/p to yield

$$\frac{e_s}{p} = \frac{q_{\mathrm{vs}}}{E + \varepsilon^{1+\alpha} q_{\mathrm{vs}}} \qquad i.e. \qquad \left(\frac{e_s}{p}\right)^{(0)} = \frac{q_{\mathrm{vs}}^{(0)}}{E}. \tag{182}$$

After division of (181) by $q_{\mathrm{vs}}^{(0)}$ and reordering terms, we find

$$\begin{aligned}&\frac{\mathrm{d}}{\mathrm{d}z}\left(\frac{q_{\mathrm{vs}}^{(1)}}{q_{\mathrm{vs}}^{(0)}}\right) - AL\frac{\mathrm{d}\theta^{(2)}}{\mathrm{d}z} - \frac{AL\Gamma - 1}{\Gamma}\frac{\mathrm{d}\pi^{(2)}}{\mathrm{d}z} \\ &= (1-\alpha)\frac{1}{E}\frac{\mathrm{d}q_{\mathrm{vs}}^{(0)}}{\mathrm{d}z} - \frac{\mathrm{d}}{\mathrm{d}z}\left(\frac{AL}{2}\left[(\chi+1)T^{(1)^2} + \theta^{(1)^2}\right] + \frac{AL\Gamma - 1}{2\Gamma}\pi^{(1)^2}\right)\end{aligned} \tag{183}$$

Integrating (183) w.r.t. z we obtain a first expression involving $q_{\mathrm{vs}}^{(1)}$, $\theta^{(2)}$, and $\pi^{(2)}$

$$\begin{aligned}\frac{q_{\mathrm{vs}}^{(1)}}{q_{\mathrm{vs}}^{(0)}} - AL\theta^{(2)} - \frac{AL\Gamma - 1}{\Gamma}\pi^{(2)} &= (1-\alpha)\frac{1}{E}\left(q_{\mathrm{vs}}^{(0)} - q_{\mathrm{vs}\,0}^{(0)}\right) \\ &\quad - \frac{AL\Gamma - 1}{2\Gamma}\pi^{(1)^2} - \frac{AL}{2}\left[(\chi+1)T^{(1)^2} + \theta^{(1)^2}\right].\end{aligned} \tag{184}$$

A second relation between these variables follows from division of (170) by $\mathrm{d}q_{\mathrm{vs}}^{(0)}/dz$ and solving for the combination $\theta^{(2)} + Lq_{\mathrm{vs}}^{(1)}$ as a function of $q_{\mathrm{vs}}^{(0)} \equiv q$,

$$\frac{\mathrm{d}}{\mathrm{d}q}\left(\theta^{(2)} + Lq_{\mathrm{vs}}^{(1)}\right) = L\left(-(1+\chi)\Gamma z + \chi\theta^{(1)} + (1-\alpha)k_v\, q\right) + (1-\alpha)\kappa_v\frac{AL^2 q + 1}{AL\Gamma - 1} \tag{185}$$

where we have used that $T^{(1)} = \theta^{(1)} - \Gamma z$ and recalled (177). The right-hand side can be integrated analytically. The terms involving $\theta^{(1)}$ and z are,

$$\int_{q_0}^{q_1}\theta^{(1)}\mathrm{d}q = -L\int_{q_0}^{q_1}(q - q_0)\mathrm{d}q = -L\left(\frac{q^2}{2} - q_0 q\right)_{q_0}^{q_1} = -\frac{L}{2}(q_1 - q_0)^2 \tag{186}$$

$$\begin{aligned}\int_{q_0}^{q_1} z\,\mathrm{d}q &= -\frac{1}{AL\Gamma - 1}\int_{q_0}^{q_1}\left[\ln\left(\frac{q}{q_0}\right) + AL^2(q - q_0)\right]\mathrm{d}q \\ &= -\frac{q_0}{AL\Gamma - 1}\left(\frac{q}{q_0}\left[\ln\left(\frac{q}{q_0}\right) - 1\right] + 1 + \frac{AL^2 q_0}{2}\left(\frac{q}{q_0} - 1\right)^2\right)\end{aligned} \tag{187}$$

where we have used the leading order expression for $q_{\rm vs}^{(0)}(z)$ from (178). The other terms are trivially integrated. This yields

$$\begin{aligned}\theta^{(2)} + Lq_{\rm vs}^{(1)} = {} & \frac{\chi}{2}L^2\left(q_{\rm vs}^{(0)} - q_{\rm vs\,0}^{(0)}\right)^2 \\ & + \frac{(1+\chi)\Gamma L}{AL\Gamma - 1}\left(q_{\rm vs}^{(0)}\left[\ln\left(\frac{q_{\rm vs}^{(0)}}{q_{\rm vs\,0}^{(0)}}\right) - 1\right] + 1 + \frac{AL^2}{2}\left(q_{\rm vs}^{(0)} - q_{\rm vs\,0}^{(0)}\right)^2\right) \\ & + (1-\alpha)\frac{Lk_v}{2}\left(q_{\rm vs}^{(0)} - q_{\rm vs\,0}^{(0)}\right)^2 \\ & + (1-\alpha)\frac{\kappa_v}{AL\Gamma - 1}\left(\frac{AL^2}{2}\left(q_{\rm vs}^{(0)} + q_{\rm vs\,0}^{(0)}\right) + 1\right)\left(q_{\rm vs}^{(0)} - q_{\rm vs\,0}^{(0)}\right). \end{aligned} \tag{188}$$

An explicit equation for $\pi^{(2)}$ is obtained by integrating (171). We replace $\theta^{(1)}$ in this equation with the result from (179), divide by $\mathrm{d}q_{\rm vs}^{(0)}/\mathrm{d}z$ and seek $\pi^{(2)}$ as a function of $q_{\rm vs}^{(0)}$. This produces, abbreviating again $q_{\rm vs}^{(0)} \equiv q$,

$$\begin{aligned}\frac{\mathrm{d}\pi^{(2)}}{dq} &= \Gamma\frac{AL^2q+1}{AL\Gamma-1}\left(L\left(1-\frac{q_0}{q}\right) - (1-\alpha)\frac{1}{E}\right) \\ &= \frac{\Gamma}{AL\Gamma-1}\left[AL^2q+1\right]\left(\frac{LE-(1-\alpha)}{E} - \frac{Lq_0}{q}\right) \\ &= \frac{\Gamma}{AL\Gamma-1}\left(AL^2\frac{LE-(1-\alpha)}{E}q + \left[\frac{LE-(1-\alpha)}{E} - AL^3q_0\right] - \frac{Lq_0}{q}\right) \end{aligned} \tag{189}$$

Integration yields

$$\pi^{(2)} = \frac{\Gamma}{AL\Gamma-1}\left(\frac{\beta_1}{2}\left(q_{\rm vs}^{(0)2} - q_{\rm vs\,0}^{(0)2}\right) + \beta_0\left(q_{\rm vs}^{(0)} - q_{\rm vs\,0}^{(0)}\right) + \beta_{-1}\ln\left(\frac{q_{\rm vs}^{(0)}}{q_{\rm vs\,0}^{(0)}}\right)\right) \tag{190}$$

where

$$\beta_1 = AL^2\frac{LE-(1-\alpha)}{E}, \quad \beta_0 = \frac{LE-(1-\alpha)}{E} - AL^3q_0, \quad \beta_{-1} = -Lq_0. \tag{191}$$

Equations (184), (188), and (190) together determine $\theta^{(2)}$, $\pi^{(2)}$, and $q_{\rm vs}^{(1)}$. For completeness, we note that

$$T^{(2)} = \theta^{(2)} + \pi^{(2)} + \theta^{(1)}\pi^{(1)} \tag{192}$$

and this completes the first-order solution for the moist adiabat.

References

1. Klein, R., Majda, A.J.: Systematic multiscale models for deep convection on mesoscales. Theor. Comput. Fluid Dyn. **20**, 525–551 (2006)
2. Kessler, E.: On the distribution and continuity of water substance in atmospheric circulations. Meteor. Monogr. **10**, 82–84 (1969)
3. Cotton, W.R., Bryan, G., van den Heever, S.C.: Storm and Cloud Dynamics, 2nd edn. Academic Press, Cambridge (2011)
4. Durran, D.R., Klemp, J.B.: The effects of moisture on trapped mountain lee waves. J. Atmos. Sci. **39**, 2490–2506 (1982)
5. Emanuel, K.A.: Atmospheric Convection. Oxford Univ. Press, Oxford (1994)
6. Grabowski, W., Smolarkiewicz, P.K.: Two-time-level semi lagrangian model for preciptating clouds. Mon. Weather Rev. **124**, 487–497 (1996)
7. Klemp, J.B., Wilhelmson, R.B.: The simulation of three-dimensional convective storm dynamics. J. Atmos. Sci. **35**, 1070–1096 (1978)
8. Klein, R.: Scale-dependent asymptotic models for atmospheric flows. Ann. Rev. Fluid Mech. **42**, 249–274 (2010)
9. LeMone, M.A., Zipser, E.J.: Cumulonimbus vertical velocity events in gate. Part 1: diameter, intensity and mass flux. J. Atmos. Sci. **37**, 2444–2457 (1980)
10. Riehl, H., Malkus, J.S.: On the heat balance in the equatorial trough zone. Geophysica **6**, 503–538 (1958)
11. Holton, J.R., Hakim, G.J.: An Introduction to Dynamical Meteorology, 5th edn. Elsevier Academic press, Amsterdam (2013)
12. Zipser, E.J.: Some views on hot towers after 50 years of tropical field programs and 2 years of TRMM data. Meteorol. Monogr. **29**(51), 49–58 (2003)
13. Leary, C.A., Houze, R.A.: The contribution of mesoscale motions to the mass and heat fluxes of an intense tropical convective system. J. Atmos. Sci. **37**, 784–796 (1980)
14. Ruprecht, D., Klein, R.: A model for nonlinear interactions of internal gravity waves with saturated regions. Met. Zeitschr. **20**(2), 243–252 (2011)
15. Ruprecht, D., Klein, R., Majda, A.: Modulation of internal gravity waves in a multi-scale model for deep convection on mesoscales. J. Atmos. Sci. **67**, 2504–2519 (2010)

16. Held, I.M., Hoskins, B.J.: Large-scale eddies and the general circulation of the troposphere. Adv. Geophys. **28**, 3–31 (1985)
17. Sobel, A., Nilsson, J., Polvani, L.: The weak temperature gradient approximation and balanced tropical moisture waves. J. Atmos. Sci. **58**, 3650–3665 (2001)
18. Liu, C., Moncrieff, W.M., Zipser, E.J.: Dynamical influence of microphysics in tropical squall lines: a numerical study. Mon. Weather Rev. **125**, 2193–2210 (1997)
19. Hernandez-Duenas, G., Majda, A.J., Smith, L.M., Stechmann, S.N.: Minimal models for precipitating turbulent convection. J. Fluid Mech. **717**, 576–611 (2013)
20. Grabowski, W.: Impact of ice microphysics on multiscale organization of tropical convection in two-dimensional cloud-resolving simulations. Q. J. R. Met. Soc. **129**, 67–81 (2003)
21. Bannon, P.R.: Theoretical foundations for models of moist convection. J. Atmos. Sci. **59**, 1967–1982 (2002)
22. Ooyama, K.V.: A dynamic and thermodynamic foundation for modeling the moist atmosphere with parameterized microphysics. J. Atmos. Sci. **58**, 2073–2102 (2001)
23. Thuburn, J.: Use of the Gibbs thermodynamic potential to express the equation of state in atmospheric models. Q. J. R. Meteorol. Soc. **143**, 1185–1196 (2017)
24. Allaby, M.: The Facts On File Weather and Climate Handbook. Facts on File (2001)
25. Carqué, G., Owinoh, A., Klein, R., Majda, A.J.: Asymptotic scale analysis of precipitating clouds. Technical report, Zuse Institut Berlin (2008)
26. Sui, C.H., Tsay, C.T., Li, X.: Convective–stratiform rainfall separation by cloud content. J. Geophys. Res **112**, D14,213 (2007). doi:10.1029/2006JD008082
27. Crandall, M.G., Lions, P.L.: Two approximations of solutions of Hamilton–Jacobi equations. Math. Comput. **43**(167), 1–19 (1984)